Lamarche-Gagnon, G., Wadham, J., Sherwood Lollar, B., Arndt, S., Fietzek, P., Beaton, A., Tedstone, A., Telling, J., Bagshaw, E., Hawkings, J., Kohler, T., Žárský, J. D., Mowlem, MC., Anesio, A., & Stibal, M. (2019). Greenland melt drives continuous export of methane from the ice-sheet bed. *Nature*, *565*(7737), 73-77. https://doi.org/10.1038/s41586-018-0800-0

Greenland melt drives continuous export of methane from its bed

Guillaume Lamarche-Gagnon[1*], Jemma L. Wadham[1], Barbara Sherwood Lollar[2], Sandra Arndt[3], Peer Fietzek[4], Alexander D. Beaton[5], Andrew J. Tedstone[1], Jon Telling[6], Elizabeth A. Bagshaw[7], Jon R. Hawkings[1], Tyler J. Kohler[8], Jakub D. Zarsky[8], Matthew C. Mowlem[5], Alexandre M. Anesio[9], Marek Stibal[8]

[1]School of Geographical Sciences, University of Bristol, Bristol BS8 1SS, UK
[2]Department of Earth Sciences, University of Toronto, Toronto, M5S 3B1, Canada
[3]Department of Geoscience, Environment & Society, Université Libre de Bruxelles, Brussels, Belgium
[4]Kongsberg Maritime Contros GmbH, Kiel 24148, Germany
[5]National Oceanography Centre, Southampton SO14 3ZH, UK
[6]School of Natural and Environmental Sciences, Newcastle University, Newcastle NE1 7RU, UK
[7]School of Earth and Ocean Sciences, Cardiff University, Cardiff, CF10 3AT, UK
[8]Department of Ecology, Faculty of Science, Charles University, Prague, 128 44, Czechia
[9]Department of Environmental Sciences, Aarhus University, 4000 Roskilde, Denmark

Abstract

Ice sheets are currently ignored in global methane budgets[1,2]. They have been proposed to cap large reserves of methane that may contribute to a rise in atmospheric methane concentrations if released during periods of rapid ice retreat[3,4], but no data on the current methane footprint of ice sheets currently exist. Here we find that subglacially-produced methane is rapidly flushed to the ice margin by the efficient drainage system of a subglacial catchment of the Greenland Ice Sheet. We report the continuous export of methane-supersaturated waters ($CH_{4(aq)}$) from the ice sheet bed during the melt season. Pulses of high $CH_{4(aq)}$ concentrations coincided with supraglacially-forced subglacial flushing events, confirming a subglacial source and highlighting the influence of melt on methane export. Sustained methane fluxes over the melt season were indicative of subglacial methane reserves in excess of export, with an estimated 6.3 (2.4 – 11) tonnes of $CH_{4(aq)}$ laterally transported from the ice sheet bed. Stable isotope analyses revealed a microbial origin for methane; most likely derived from a mixture of inorganic and ancient organic carbon buried beneath the ice. We show that subglacial hydrology is crucial for controlling methane fluxes from the ice sheet, with efficient drainage limiting the extent of methane oxidation[5] to about 17% of methane exported. Atmospheric evasion is the main methane sink once runoff reaches the ice margin, with estimated diffusive

fluxes (4.4 – 28 mmol-CH_4 m^{-2} d^{-1}) rivalling that of other world rivers[6]. Overall, our results provide evidence that ice sheets overlay extensive, biologically active methanogenic wetlands, and that high rates of methane export to the atmosphere can occur where efficient subglacial drainage pathways exist. Our findings suggest that such environments should be considered a previously underappreciated component of Earth's methane budget.

The role of ice sheets in the global methane cycle depends on the ability (thermogenic or microbial) of subglacial environments to evolve large quantities of methane (e.g. as hydrates) [3,4,7], as well as the mechanisms responsible for methane export to the ice margin and subsequent release to the atmosphere. Subglacial CH_4-hydrates have been suggested to currently exist beneath the Antarctic Ice Sheet, large enough to raise atmospheric methane concentrations if released rapidly during deglaciation[4]. However, recent research has revealed the presence of active methane-oxidizing communities in subglacial ecosystems, suggesting the possibility of an efficient methane buffer by an active biological sink[5,8]. There is also ambiguity in the paleo-record. New ice core data suggests that geological methane (e.g. from permafrost, but also potentially of ice sheet origin) had little role in affecting atmospheric methane concentrations over the Younger Dryas-Preboreal transition[9]; but previous estimates do suggest large subglacial methane releases from retreating Paleo-ice sheets of the Northern Hemisphere following the onset of the last deglaciation[10]. Confounding scenarios on the potency of sub-ice-sheet methane mostly result from the scarcity of empirical data, limited to point measurements in ice cores[11-13], Greenland marginal streams[5], and an Antarctic subglacial lake[8].

Here we provide direct evidence from the GrIS for the existence of large subglacial methane reserves, where production is not offset by local sinks and there is net export of methane to the atmosphere during the summer melt season. We focused on a 600 km^2 catchment of the GrIS which has been extensively studied over the last decade, both in terms of ice dynamics and subglacial geochemistry (Supplementary Information 1a). Between 19 May and 13 July 2015, we deployed a CONTROS HydroC® CH_4 sensor[14] (Kongsberg Maritime Contros, Germany) < 2 km of the ice margin in the proglacial river of the Leverett Glacier (LG) (Supplementary Information 1.a; Extended Data Fig. 1)[15,16]. Manual measurements supported sensor readings and CH_4 stable isotope analyses ($\delta^{13}C$ and $\delta^{2}H$) and 16S rRNA gene sequence data from LG runoff were employed to infer methane origin. A one dimensional reaction-transport model

was further applied to test for the possibility of hydrate formation beneath the ice in the catchment. Features of the study area suggest that results obtained are likely to be applicable to other ice-sheet catchments (Supplementary Information 1a), and are informative on a global scale, serving as a first-step assessment of subglacial methane contribution to present-day methane budgets.

Sensor measurements revealed that LG runoff was supersaturated in methane with respect to the atmosphere over the entire monitoring period (mean concentration of ~271 nM, compared with an atmospheric equilibrium concentration of ~ 4.5 nM) (Fig. 1). This is consistent with the high concentrations (up to ~24 µM) of methane detected in the basal regions of the GRIP, GISP2, and NGRIP ice cores[11-13], in marginal runoff from a small neighbouring Greenland glacier (~3-83 µM)[5] and during experimental incubations of Greenland subglacial sediment[17]. Stepwise increases in methane concentrations closely followed the seasonal evolution of the subglacial drainage system, indicating the crucial role of hydrology in controlling methane export from the ice sheet. Clear differences in $CH_{4(aq)}$ concentrations were observed between a) the early part of the season during times of very low discharge when the subglacial portal was completely ice-sealed, and methane concentrations were low (mean ~64 nM) (Fig.1, Supplementary section 2b), b) the emergence of a subglacial upwelling through the river ice in front of the LG on June 1, which released over-winter stored waters enriched in methane from the ice margin (mean ~4 µM prior to the melt season; see Supplementary Information 1b, Extended data Fig. 1), and c) the later season (from June 19 onwards) with elevated $CH_{4(aq)}$ concentrations (pulses) coincident with a series of four subglacial outburst events (Supplementary Information 2b; Fig. 1). These outburst events were characterised by pulses in suspended sediment concentrations (SSC), electrical conductivity (EC), and pH (Fig. 1), indicative of subglacial origin as previously inferred[18]. The high concentrations of $CH_{4(aq)}$ observed during these events suggest the evacuation of methane-rich subglacial waters from progressively up-glacier sources (Supplementary Information 2b). We attribute the overall decreasing trend in methane concentration following the second outburst event to dilution by rising supraglacial icemelt inputs to the subglacial system over the melt-season. The sustained methane load observed during this period, however, indicates that subglacial methane reserves are not exhausted despite increases in meltwater discharge (Fig. 1).

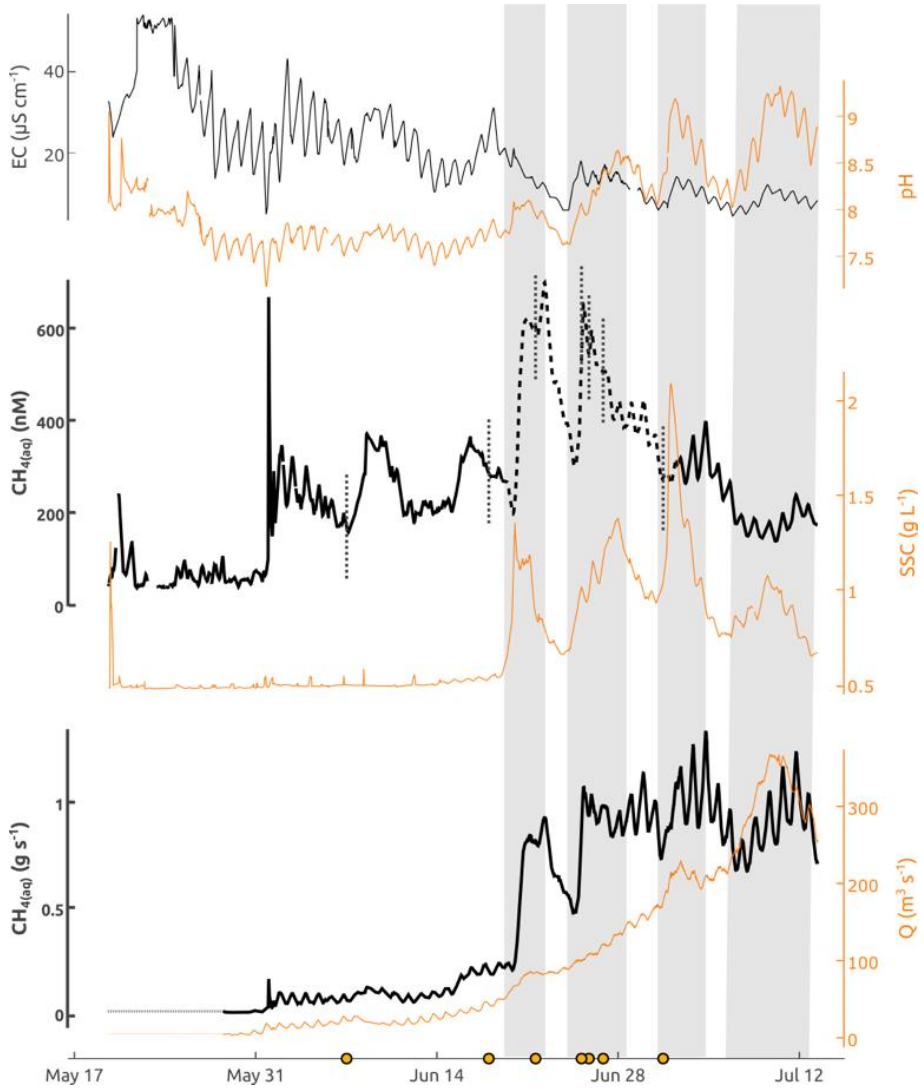

Fig. 1 **Geochemical time series of the LG proglacial river** – Top: Electrical-conductivity (EC) and pH. Middle: $CH_{4(aq)}$ (HydroC®) and suspended sediment concentrations (SSC); the dashed section corresponds to times when the HydroC® sensor experienced slower response times (see Supplementary Information 2a, Extended Data Fig. 2). Orange dots and vertical dashed lines indicate sampling time of waters used for stable isotope analysis (see Extended Data Table 2). Bottom: $CH_{4(aq)}$ lateral flux and discharge (Q); the first data points on May 28 are extended to the first data point of the above sensor measurements (dashed horizontal lines). Abrupt increases in SSC, EC, pH, and $CH_{4(aq)}$ correspond to outburst events (shaded sections) and reflect sudden drainage of sub-ice sheet waters and sediments driven by supraglacial melt water entering the subglacial system (Supplementary Information 2b). Y axes corresponding to black and orange datasets are located on the left and right, respectively.

The cumulative lateral flux of $CH_{4(aq)}$ from LG amounted to ~1.87 (1.64 – 2.10) tonnes (t) over the measurement period. However, we estimate that at least 2.78 (2.43 – 3.12), but more likely ~6.28 (5.19 – 7.36) t of $CH_{4(aq)}$, were laterally transported at the measuring site over the entire 2015 melt season (Fig. 2, see methods for details). Methane measurements provide

conservative estimates of total methane production across the glacier, since recorded concentrations would have been influenced by oxidative and diffusive processes upstream of the measuring site, and hence subglacial methane production beneath the catchment are likely larger. Based on previously measured microbial oxidation rates[5], we estimate that the bacterial methane sink at LG to have amounted to ~ 1.22 t prior to subglacial discharge reaching the ice margin, or about 16% of total methane export at the measuring site over the melt season on the basis of a sustained flux scenario (Fig. 2; Supplementary Information 2c).

We employ scaling relationships between gas transfer velocities and river hydrology[19] to derive conservative approximations of diffusive fluxes of methane from the LG proglacial river. We infer that there will be some evasion of methane from subglacial runoff to air spaces in subglacial channels close to the margin[20] and to the atmosphere after emergence at the glacier subglacial portal. We estimate that such atmospheric evasion constitutes the main sink of $CH_{4(aq)}$ when compared to microbial oxidation, with diffusive fluxes responsible for at least 1.72 (0.51 – 3.19) t of CH_4 released to the atmosphere between the ice margin and the measuring site (Fig. 2; compared to ~ 0.09 t of CH_4 oxidised for the same distance, or ~ 1% of exports, data not shown). Recent work on white-water streams have indicated that these traditionally used scaling relationships can grossly underestimate (by several orders of magnitude) diffusive fluxes in white-water systems[21,22]. Considering the high degree of turbulence observed on the LG river (Extended Data Fig. 1), we therefore stress that our estimates here constitute lower limit values. What is clear is that the LG catchment is a source of atmospheric methane, with our minimum estimates indicating that over 18% (7.5 – 26%) of exported methane reaches the atmosphere within 2 km of the ice sheet margin.

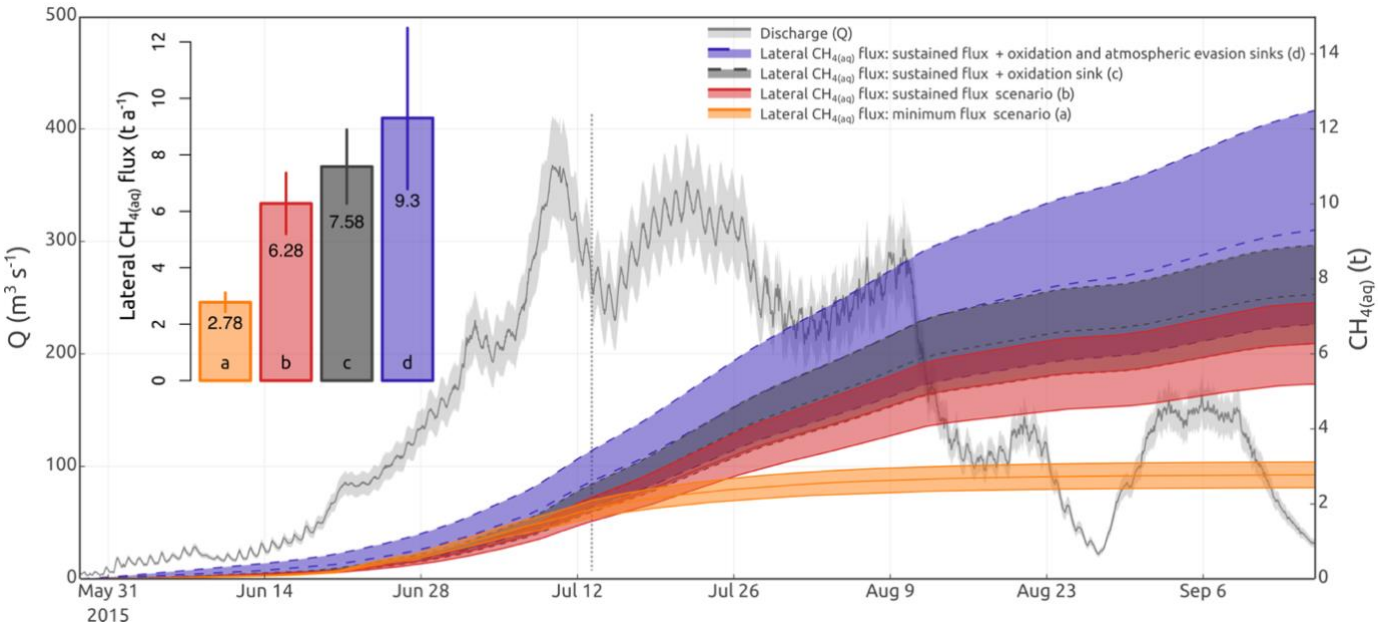

Fig. 2 **Cumulative lateral export of LG $CH_{4(aq)}$ over the 2015 melt season – Cumulative lateral export of LG $CH_{4(aq)}$ over the 2015 melt season.** Orange and red lines correspond to the minimum and sustained methane flux scenarios, respectively, at the measuring site (see Methods). Dark-grey lines represent a scenario that accounts for a methanotrophic methane sink on a sustained-flux scenario and represent the expected lateral methane flux that would have occurred without a methanotrophic sink. Blue lines correspond to a scenario that accounts for the combined estimated methanotrophic and diffusive flux sinks of methane before reaching the measuring site, added to a sustained-flux scenario. The vertical dotted line marks the last day of $CH_{4(aq)}$ sensor measurements (13 July). The width of the shaded areas corresponds to errors from sensor measurements and estimates of gas transfer velocities (see Methods). The pale-grey time series denotes discharge measurements over the entire melt season. The annual methane fluxes depicted in the bar plot correspond to the cumulative fluxes at the end of the melt season for each of the estimated scenarios; error bars correspond to the range depicted by the shaded areas.

Methane concentrations at LG fell within the global range reported for streams and rivers (Fig. 3). A recent survey of riverine methane indeed revealed that streams have previously been overlooked as net contributors of atmospheric methane, estimated to emit over 27 Tg of CH_4 annually, or ~ 15-40% of global wetland and lake effluxes respectively[6]. Results presented here suggest that streams draining subglacial basins are probably no exception, with the estimated diffusive fluxes of methane at LG falling in the higher range of reported world averages for rivers, comparable to the large fluxes observed in the Congo basin (Fig. 3; Extended data Table 1). Because of the high uncertainties surrounding LG methane diffusive fluxes, it is difficult to accurately determine the overall contribution of methane to the atmosphere from the LG catchment, and by extension from the GrIS margin as a whole.

In order to more directly compare methane fluxes at LG with other systems, we calculated a catchment-wide areal yield of $CH_{4(aq)}$ that contributed to the observed $CH_{4(aq)}$ lateral flux. When comparing catchment area-normalised yields of $CH_{4(aq)}$, the lateral $CH_{4(aq)}$ flux from LG translates into a yield significantly higher than, or within the range, of other large rivers worldwide, and highlight that the GrIS may act as a relatively important source of atmospheric methane (Extended Data Table 1, Supplementary Information 1c). Ultimately, the atmospheric footprint of GrIS CH_4 will partly depend on the overall surface area of the ice sheet contributing to the overall diffusive fluxes, as well as the magnitude of such fluxes at points of first contact between the atmosphere and subglacial runoff (e.g. within open channels beneath the ice).

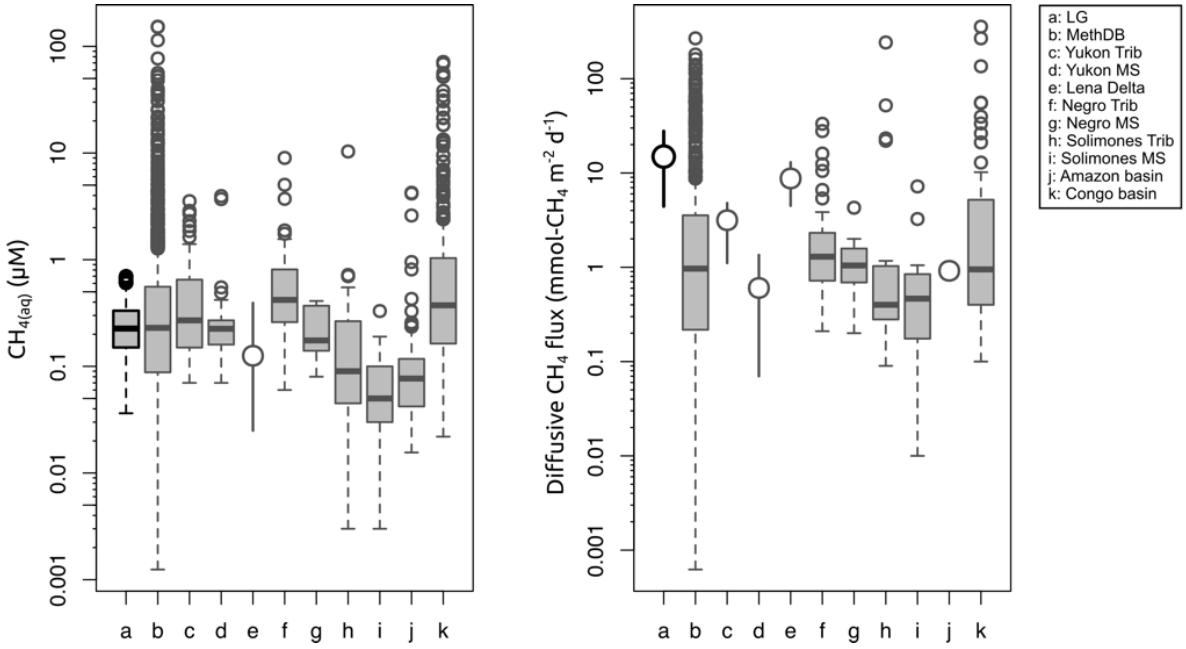

Fig. 3 **Box plots of $CH_{4(aq)}$ concentrations and diffusive fluxes for the LG and other major world river systems** – Box mid lines represent medians; the interquartile range (IQR) is represented by the lower and upper box boundaries and denote the 25th and 75th percentiles, respectively; whiskers indicate 1.5 times IQR confidence intervals and points are outliers. Where no raw data was available, averages and reported ranges are depicted by circles and error bars (see Supplementary Information 1c for details). MethDB refers to a worldwide $CH_{4(aq)}$ dataset for rivers[6]. "Trib" and "MS" refer to rivers' tributaries and mainstems, respectively.

Stable isotope analyses ($\delta^{13}C$ and $\delta^{2}H$) revealed that LG methane was microbial in origin, with most samples falling in a well-defined range characteristic of acetoclastic methanogenesis, although with some degree of mixing with methane likely produced by a CO_2-reduction

pathway *(*Fig. 4). This mixed origin of methane by CO_2-reduction and acetate fermentation is also supported by molecular evidence from the LG proglacial stream, which identified the presence of 16S rRNA gene sequences related to both hydrogenotrophic and acetoclastic methanogens (Extended Data Fig. 4; Supplementary Information 2d). A mixed methane source at LG suggests the availability of several methanogenic substrates beneath the ice, likely derived from the recycling of overridden old carbon (e.g. acetate), such as seen in GrIS marginal lakes[23], potentially supplemented by H_2 gas generated from rock comminution hypothesised to fuel methanogens beneath ice masses over extended glaciation[24] (see Supplementary Information 2.d).

Partial oxidation during transit from the subglacial system likely enriched the sampled methane with heavier stable isotopes[25] (Supplementary Information 2c), yet there is no strong isotopic trend that conclusively identifies methanotrophy as a major control on the isotopic signatures observed here (Fig. 4; Extended Data Fig. 3). This contrasts with patterns we observed for stagnant waters beneath the LG proglacial river-ice (this study, Extended Data Fig. 3) and waters sampled from Antarctic Subglacial Lake Whillans (Supplementary Information 2c). We infer the limited methanotrophic signature here to reflect the largely anoxic conditions at the sites of methane production (and thus limited aerobic oxidation of methane) and the rapid evacuation of methane from the production site via a fast and efficient drainage system (Supplementary Information 2b).

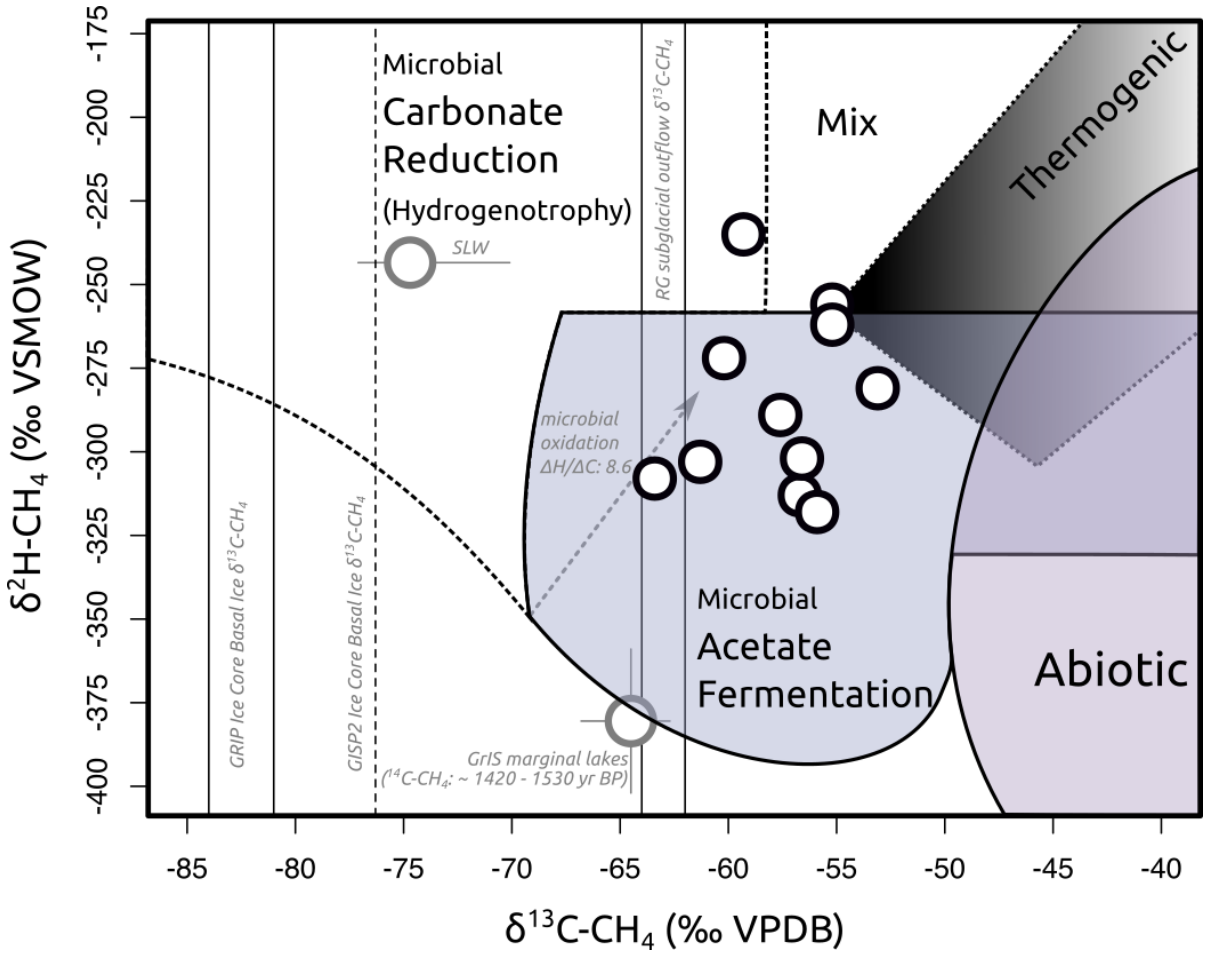

Fig. 4 **Carbon-Hydrogen isotopic diagram of LG $CH_{4(aq)}$** – Black-border points denote dual stable-isotope values ($\delta^{13}C$ and $\delta^{2}H$) for LG $CH_{4(aq)}$ samples (sample values are summarized in Extended Data Table 2). Average $\delta^{13}C$- and $\delta^{2}H$-CH_4 values and ranges from Subglacial Lake Whillans (SLW) in Antarctica[3] and GrIS marginal lakes[24] are added as references (grey-border points), as well as $\delta^{13}C$-CH_4 data from GrIS ice-core basal ice[12,23] and from the subglacial outflows of the Greenland Russell Glacier (RG)[6] (marked by vertical lines). The estimated carbon age (years before present – yr BP) from ^{14}C analyses of the GrIS marginal lakes methane[24] is indicated next to point. The arrow denotes the microbial oxidation effect on CH_4 stable-isotope signatures; $\Delta H/\Delta C$ denotes the gradient (delta $\delta^{2}H$-CH_4 over delta $\delta^{13}C$-CH_4) of the arrow[26]. The classification zones and definitions of methane origins are derived and adapted from refs [25,26]. VSMOW, Vienna standard mean ocean water; VPDB, Vienna Pee Dee belemnite.

The impact of subglacial methane on atmospheric concentrations partially depends on the presence of methane hydrates beneath ice sheets, as catastrophic CH_4-hydrate destabilization during periods of rapid ice thinning could likely result in very large fluxes of methane to the atmosphere[3,4]. We employed a 1D reaction-transport model to identify the conditions required to allow for CH_4-hydrate formation beneath the LG catchment. Our results indicate that relatively high methanogenic rates (larger than observed in Greenland basal ice incubation

experiments[17]; Extended Data Fig. 5) and thick sediment layers (at least several tens of meters) are required to evolve and sustain methane hydrates beneath the LG catchment (Supplementary Information 2e, f). The high methane flux that would be generated at the ice-sediment interface under CH_4-hydrate conditions (estimated at 10 to 1,000 times larger than the observed lateral flux depending on hydrate conditions; Extended Data Fig. 6) makes it unlikely that a significant portion (if any) of the exported CH_4 measured from the LG comes from subglacial CH_4-hydrates. Importantly, however, the model results suggest that conditions favourable to hydrate formation are likely present in other regions of the GrIS, where there has been sustained thick ice cover (e.g. for > 10,000 years), and where thick sedimentary layers exist (e.g. ref. [27]; Supplementary Information 2f).

Using high-resolution *in situ* sensor measurements, we show that an extensive area of the GrIS continuously releases methane-supersaturated runoff from its bed during the melt season. Our results constitute the first measurements of sustained methane export from an ice sheet catchment, and highlight the need to better gauge the footprint of ice sheets on current methane budgets. The release of several tonnes of microbial methane from beneath the GrIS represents one of the strongest lines of evidence to date for significant microbial production of methane in subglacial ecosystems, and reinforces the view that large methane reserves may accumulate beneath past and present day ice sheets[3,7]. This methane can reach the atmosphere where fast-flowing drainage networks enable its rapid transport beyond the ice margin prior to being oxidised to carbon dioxide, whether driven by supraglacial forcing in the GrIS ablation zone, or potentially also during episodic subglacial lake drainage events in Antarctica[28]. The influence of meltwater discharge on methane export observed here further suggests that projected increases in warming and melting rates could also lead to increases in subglacial methane release to the atmosphere. Our findings that subglacial environments in Greenland can generate high levels of methane emphasise the need to directly measure methane reserves in subglacial systems containing high quantities of organic carbon, such as the thick sedimentary basins beneath the Antarctic Ice Sheet, where much larger amounts of methane, as hydrates, are expected to be present[4].

Acknowledgments

We thank all of those who assisted with fieldwork at LG, especially Jade Hatton, as well as Dr Fotis Sgouridis and Mr James Williams in LOWTEX laboratories at the University of Bristol. This research is part of the UK NERC funded DELVE programme (NERC grant

NE/I008845/1) to J.L. Wadham and G. Lamarche-Gagnon was funded via the University of Bristol Scholarship Program and FRQNT Scholarship (scholarship ID 185136) for his PhD. The work was also supported via Leverhulme Trust, via a Leverhulme research fellowship to JLW, a UK NERC grant (NE/J02399X/1) to A.M. Anesio for DNA analyses, as well as Czech Science Foundation grants (GACR; 15-17346Y and 18-12630S) to M. Stibal. Isotopic analyses were conducted by Dr. Georges Lacrampe-Couloume at the University of Toronto with support provided by the Natural Sciences and Engineering Research Council of Canada (NSERC) to B.S.L. We also thank the Kangerlussuaq International Science Station, especially Rikka Møller, for support with field logistics, as well as Michael A. Cooper, Moya Macdonald, and Stefan Hoffer for comments.

Author contribution

J.L.W. and G.L.G. designed the study. B.S.L. supervised stable-isotope analyses. S.A. performed the reaction-transport hydrate model calculations. P.F. assisted in the interpretation and analysis of the CONTROS HydroC®-CH_4 raw results. G.L.G., J.T., E.A.B., A.D.B., M.C.M. and J.R.H. conducted field logistical preparations. J.L.W., J.T. and M.S. led the 2015 Greenland field campaign. G.L.G., A.D.B., A.J.T., J.T., E.A.B., J.R.H., T.J.K., J.D.Z. and M.S. collected the sensor field data. G.L.G. and J.D.Z. collected manual water samples in the field. G.L.G. and A.M.A. analysed molecular data. G.L.G. performed the data analysis and wrote the manuscript with significant contribution from all co-authors.

Data availability

The data used in this article are available from the corresponding author (guillaume.lg@bristol.ac.uk) on request. The 16S rRNA gene sequence data are available in the NCBI Sequence Read Archive (https://www.ncbi.nlm.nih.gov/sra) under BioProject PRJNA495593 (BioSamples SAMN10228172-SAMN10228185; SAMN10228190-SAMN10228206).

Author information

Original article available at doi: 10.1038/s41586-018-0800-0

Correspondence to guillaume.lg@bristol.ac.uk.

Competing interests

P.F. works for the sensor manufacturer but the discussed sensor data was validated by independent measurements. The remaining authors declare no competing interests.

METHODS

Site description and hydrogeochemical analyses

The hydrology of LG has been extensively studied and described previously (see Supplementary Information 1a). A detailed description of the proglacial study site, as well as the hydrological and geochemical monitoring performed during the 2015 melt season can be found in two parallel studies[16,29]. Briefly, a suite of hydrogeochemical sensors [logging for pH, (Honeywell Durafet), water temperature (Aanderaa and Campbell Scientific), electrical conductivity (Campbell Scientific 547), and turbidity (Partech C)] were deployed in the LG proglacial river ~ 1.6 km downstream from the subglacial ice portal at the glacier's terminus (Extended Data Fig. 1). Turbidity measurements were converted to suspended sediment concentrations by calibration against manual sediment samples collected over the span of the melting season as per ref. [30]. Discharge measurements were derived from pressure transducers (Druck and Hobo) and stage sensors (Campbell Scientific SR50A) fixed in a bedrock section ~ 2 km downstream from the glacier's terminus. Stage measurements were converted to discharge using a stage-discharge rating curve generated from calibration against repeat Rhodamine dye injections over the full range of river stages during the melt season as per ref. [18]. Uncertainties (RMSD) on discharge measurements were calculated to be ~ 12.1%.

Manual sampling

Manual samples were collected a few meters (~ 5-10 m) upstream of the HydroC®. Water samples were collected inside pre-evacuated (at most 500 mTorr) 120 mL borosilicate vials sealed with 2 cm thick butyl-rubber stoppers, pre-flushed with 5.0 grade argon, and pre-poisoned with ~24 mg of $HgCl_2$ to fix the samples and prevent any microbial activity affecting the gases post-sampling; after the method of ref. [31]. 10 mL (at room temperature and pressure) of helium (grade 5.0) was added to the evacuated vials to maintain a headspace during sampling. Most water samples (n=53) were collected using a peristaltic pump (Portapump-810, Williamson Manufacturing) equipped with silicone tubing; a small number of samples were collected using plastic syringes (n=2) or passively using the vials' vacuum pressure by directly piercing the septum of submerged vials with a needle (n=8). Vials containing apparent air contamination or vacuum loss (e.g. resulting in abnormally large headspace post sampling)

were excluded from analyses. Samples for stable isotopic analysis were collected as above (n=9 collected using the peristaltic pump, n=2 using syringes).

Methane concentrations were calculated using the headspace method. Headspace samples were analysed on an Agilent 7980A gas chromatograph equipped with a Porapak Q 80-100 mesh, 2.5 m X 2.0 mm SS column and flame ionization detector. Standard curves were calculated from certified (± 5%) gas standard measurements. Gas concentrations were converted to molar concentrations using the ideal gas law and dissolved methane concentrations were obtained using Bunsen coefficients[32]. Internal vial pressures were calculated using the ideal gas law from the difference between the headspace volume post-sampling and the theoretical headspace volume of 10 mL at 1 atm and 20°C. The average internal pressure of 3.5 (± 0.9 standard deviation) atm was assigned to all manual samples for calculations.

CONTROS HydroC® CH_4 sensor

Methane measurements were performed using a CONTROS HydroC® CH_4 system (Kongsberg Maritime), an optical (infrared), headspace-based underwater sensor. An underwater pump (SBE 5T, Sea-Bird Scientific) mounted to the sensor continuously feeds water to the membrane equilibrator. Dissolved gases diffuse through a composite membrane into the internal gas circuit where partial-pressure is measured via tunable diode laser absorption technology[14]. The CONTROS HydroC® sensor was deployed completely submerged within a solid metallic cage moored by cables attached to boulders on the river bank, with the sensor head facing the river current (Extended Data Fig. 1). Measurements were logged every minute between May 19 and June 4; the logging interval was changed to 5 minutes on June 4 until the end of the measuring period on July 13.

The ideal gas law and Bunsen coefficients were used to convert µatm measurements (Extended Data Fig. 7c) to molar concentrations (Fig. 1). Water temperatures ±0.05°C were recorded using an Aanderaa Optode 3830 sensor deployed in parallel (Extended Data Fig. 7a). The CONTROS HydroC® CH_4 reported overall uncertainty is 2 µatm (~ 5nM) or ±3% of reading, whichever is greater.

Calculation of lateral methane flux

$CH_{4(aq)}$ measurements stopped on July 13. $CH_{4(aq)}$ fluxes estimated during the rest of the ablation season were based on two scenarios: i) assuming that methane levels would immediately decrease until reaching river baseline concentrations on September 15 (last discharge measurement), or alternatively, ii) continue to follow a discharge-dependent trend for the duration of the ablation season.

i. Constant concentration-decrease scenario (annual lateral flux of 2.78 t-CH_4)

In the constant concentration-decrease scenario, a baseline $CH_{4(aq)}$ concentration was set based on manual water samples collected during a return visit to the sampling site on October 28, at a time during which the proglacial river was partially frozen, and where no runoff contribution to the proglacial river stream was apparent. October concentrations averaged ~18.5 nM (beneath river ice at that time, n=6).

The minimum flux scenario was calculated using a natural log decrease behaviour of the form:

$$y=C\ e^{-(kt)}$$

where y is the methane flux (e.g. in g s^{-1}), C is the last flux measurement on July 13 (i.e. 0.71 g s^{-1}), t is the time elapsed between July 13 and the flux y, and k is the reaction constant obtained assuming a baseline concentration of 18.5 nM and using the discharge of 32 m^3 s^{-1} (last discharge measurement) on September 15.

ii. Sustained-flux scenario (annual lateral flux of 6.28 t-CH_4)

The sustained-flux scenario was calculated using the discharge-weighted mean $CH_{4(aq)}$ concentration of 271 (± 34) nM obtained from measurements up to July 13; the error reflects errors on discharge measurements (12.1%) as well as the HydroC®-CH_4 measurement errors (2 µatm or 3%, whichever is greater).

Estimation of methane sink via methanotrophic oxidation

The recorded methane concentrations at LG most likely underestimated the original methane levels present beneath the catchment because of the water travel time between the subglacial methane source and the measurement site. In addition to atmospheric evasion of methane,

aerobic microbial oxidation of methane would have lowered methane concentrations prior to reaching the observation site once fully oxygenated meltwater runoff entered the subglacial system (O_2 concentrations in runoff were either in near atmospheric equilibrium or supersaturated for most of the monitoring period; Extended Data Fig. 7a). Methanotrophy was observed qualitatively in a small number of un-fixed river samples collected in parallel to fixed manual samples, with up to a 100 fold decrease in $CH_{4(aq)}$ concentrations in unfixed versus fixed vials upon analyses back in the home laboratory (data not shown). However, no time series incubation was set-up and consequently no methanogenic rates were calculated for the LG site.

The quantity of methane oxidized by methanotrophic bacteria prior to reaching the measuring site was estimated using the methanotrophic rate reported for the marginal stream of the neighbouring Russell Glacier (i.e. 0.32 µM d^{-1})[5]. Justifications for using the Russell Glacier oxidation rate are discussed in Supplementary Information 2c. The time during which runoff was subject to methane oxidation (i.e. water travel-time) was estimated from water velocities and subglacial drainage evolution calculated based on a previous study at LG by Chandler et al. 2013 (ref. [20]). We assumed that subglacial aerobic methane oxidation occurs between the location of supraglacial runoff-input, where oxygenated supraglacial waters enter the subglacial system, and the measuring site located 1.6 km downstream of the LG glacier terminus.

Water velocities were calculated using the relationship between maximum tracer velocity (v0.5) and cumulative discharge ($\sum Q$) described for the gaseous SF6 tracer in ref. [20], which takes the form:

$$v0.5 = A * \ln(\sum Q) + B$$

with regression parameters A and B calculated to be 0.235 m s^{-1} and -3.59 m s^{-1} respectively[20]. We fixed a minimum velocity of 0.4 m s^{-1}, which corresponds to the minimum v0.5 calculated for tracer injections performed 7 km inland from the LG portal at times of low cumulative discharge by Chandler et al. 2013.

We estimate the inland evolution of an efficient channelized subglacial hydrological system based on the relationship between cumulative discharge and v0.5 at moulin injection sites (see Fig. 2.a in ref. [20]). We derived the progression of supraglacial water-inputs using the lowest

value of cumulative discharge observed where v0.5 at an injection site fell onto the regression line of v0.5 to cumulative discharge for the L7 injection in ref. [20] (see Figure S2.8 in ref. [20]). That is, we fixed that the channelized subglacial channel would reach 7 km at a cumulative discharge of 1.9 x 10^7 m^3, 14 km at a cumulative discharge of 9.4 x 10^7 m^3 and 41 km at 7.8 x 10^8 m^3 based on figure S2.8 and Table S1 in ref. [20]. We acknowledge that such calculations are approximate at best, but they allow the use of a dynamic distance of travel during the melt season. We fixed a maximum travel distance of 41 km from the LG terminus, after which the LG subglacial system is considered to become primarily inefficient and distributed for the duration of the ablation season[20]. To account for potential methane sources and methanotrophic activity occurring downstream of the supraglacial-runoff input into the subglacial channelized-system, we used an average distance of travel in our calculation (i.e. half of the distance of travel obtained from cumulative-discharge calculations above).

Calculation of diffusive methane flux

Accurately calculating methane losses due to atmospheric evasion was beyond the scope of the present study, and therefore, flux numbers should be considered conservative estimates of the amount of methane originally generated and exported from the LG catchment.

Diffusive fluxes for the LG stream were estimated following the approach by Raymond et al. 2013[19], which estimates gas transfer velocity coefficients (*k*) from stream slope and water velocity (fitted equation 5 in ref. [33]). Fluxes were estimated for the first 1.6 km of the proglacial river, from the ice margin to the measuring site. Stream slope was obtained via Google Earth and approximated 0.04; a slope value of 0.01, 0.03, and 0.05 was used to generate minimum, medium, and maximum *k* values. A water velocity of 1 m s^{-1} was used which corresponds to the discharge weighted mean of subglacial water velocities (v.05) used for methanotrophic sink calculations (see above).

Methane gas transfer velocities (k_{CH4}) were converted from the calculated k_{600} values following relationships between Schmidt numbers and *k* for CO_2 and CH_4 (see equations 2 and 3 in ref. [33]); Schmidt numbers were calculated using an average water temperature value of 0.22°C (Extended Data Fig. 7d)[34]. Minimum, medium, and maximum slope values, as we well as standard deviations on k_{600} equation parameters[33] resulted in minimum, medium, and maximum k_{CH4} of 16, 49, and 84 m d^{-1} respectively.

Methane diffusive fluxes were calculated using the discharge-weighted mean $CH_{4(aq)}$ concentration for the observation period (271 nM) and assuming an atmospheric methane concentration of 1.8 ppmv (resulting in an equilibrium concentration of about 4.6 nM). Diffusive flux occurring upstream of the measuring site was calculated using 1 m retroactive bins, adjusting upstream dissolved methane concentrations for methane loss by both diffusive flux and microbial oxidation losses in downstream bins; a fixed river width of 40 m, water velocity of 1 m s^{-1}, and average discharge of 150 m^3s^{-1} were used in calculations. The reported diffusive flux values correspond to the average flux calculated for the 1.6 km of stream for each minimum, medium, and maximum scenarios. Cumulative fluxes were calculated for the discharge-measurement period (i.e. ~ 110.5 days) and normalized to estimated water velocities (see above section). Details on the diffusive fluxes of other world rivers can be found in Supplementary Information 1c.

Stable Isotope Analyses

Analyses for $\delta^{13}C$ values were performed by continuous flow compound specific carbon isotope ratio mass spectrometry with a Finnigan MAT 252 mass spectrometer interfaced with a Varian 3400 capillary GC. Hydrocarbons were separated by a Poraplot Q™ column (25m x 0.32mm ID) with temperature program: initial 40°C hold 1 minute, increase to 190°C at 5°C/min., hold 5 minutes. Total error incorporating both accuracy and reproducibility is ± 0.5‰ with respect to V-PDB standard[35]. The δ^2H analysis was performed on a continuous flow compound specific hydrogen isotope mass spectrometer which consists of an HP 6890 gas chromatograph (GC) interfaced with a micropyrolysis furnace (1465°C) in line with a Finnigan MAT Delta$^+$-XL isotope ratio mass spectrometer. H_2 and CH_4 were seprated by a Molecular Sieve 5A column (25m x 0.32 mm ID) with a carrier gas flow rate of 1.2 mL/min with the temperature program: initial 20°C, hold for 5 minutes followed by an increase to 280°C at 25°C/min. Higher hydrocarbons were separated using the same column and temperature program as the carbon isotope analysis. Total error incorporating both accuracy and reproducibility for hydrogen isotope analysis is ± 5 ‰ with respect to V-SMOW[31].

CH_4-Hydrates

In order to evaluate the potential for hydrate formation beneath the LG catchment, we employed a one-dimensional reaction-transport model that has been originally developed for simulating hydrate formation in marine sediments[36] and has previously been adapted for

subglacial Antarctica[4]. We assumed physical properties for sediments similar to those previously employed for ocean sediment modelling[36]. Extended Data Table 3 summarizes site-specific model parameters, their model values and units. The model solves the one-dimensional diffusion-advection-reaction equations for dissolved methane, gaseous methane and methane hydrates. The implemented reaction network accounts for a constant methane production rate R_{xn} over a predefined sediment depth z_{xn}, methane hydrate, as well as methane gas formation and dissociation. At the upper boundary, the boundary concentrations are set to zero (i.e. Dirichlet boundary condition) reflecting warm-based conditions and allowing for diffusive flux of methane through the ice-sediment interface. In addition, initial conditions for dissolved and gaseous methane, as well as methane hydrates were set to zero. A "best case" scenario was designed to reflect optimal, but plausible physical and biogeochemical conditions for hydrate formation to assess the maximum potential for hydrate accumulation in the catchment. More specifically, we assigned a thick methanogenic sediment layer beneath the catchment (i.e. up to 100 metres), a 10,000 year ice sheet overburden to allow for hydrate evolution, complete anoxic conditions, an overlaying ice thickness set to 1,000 metres (ice thickness over the LG catchment exceeds 1,000 metres at ~ 39 km from the ice margin[20]), a basal temperature of -1˚C, and assumed the absence of a methane sink within the sediment layer (e.g. no anaerobic oxidation of methane). This "best case" model set-up was run over a wide range of constant methane production rates (Rxn= 10^{-17} to 10^{-13} g-CH_4 g^{-1} wet sediment s^{-1}) to determine the order of magnitude of methane production rates required to accumulate hydrates. After this initial screening, methane production rates were varied systematically between Rxn= 10^{-15} to 10^{-14} g-CH_4 g^{-1} wet sediment s^{-1}.

EXTENDED DATA

Extended Data Table 1 | $CH_{4(aq)}$ concentration, fluxes, and areal yield from LG, the GrIS, and other world rivers*

River	Catchment Area (10^6 km²)	Discharge (km³ a⁻¹)	Concentration (μM $CH_{4(aq)}$)	Diffusive flux (mmol-CH_4 m⁻² d⁻¹)	Diffusive flux (Gg-CH_4 a⁻¹)	Lateral flux (Gg-$CH_{4(aq)}$ a⁻¹)	Areal Yield Diffusive (mmol-CH_4 m⁻² a⁻¹)	Areal Yield Lateral (mmol-$CH_{4(aq)}$ m⁻² a⁻¹)
LG runoff	**0.0006**	**1.45**	**0.27**	**14.94**	**-**	**0.0063**	**-**	**0.65**
GrIS runoffs†	-	*418*‡	*0.27*	-	-	*2.1*	-	-
Lena Delta	2.49	821	0.07	9.22	150	0.9	3.8	0.02
Yukon Trib	0.19	48	0.75	3.16	12	0.6	4.0	0.19
Yukon MS	0.82	206	0.38	0.60	8	1.3	0.6	0.10
Negro Trib	0.69	455	0.87	-	-	6.0	-	1.29
Negro MS	0.69	1634	0.26	2.00	79	4.2	7.2	0.38
Solimões Trib	0.99	1985	0.33	-	-	10.6	-	1.17
Solimões MS	0.99	3507	0.06	1.60	160	3.3	10.1	0.21
Amazon	6.03	5444	0.18	0.92	490	15.5	5.1	0.16
Congo	3.71	1270	3.17	16.42	1906	64.6	32.1	1.10

*Diffusive fluxes are calculated grand means except for the LG runoff diffusive flux which corresponds to the medium flux scenario (scenario b in Fig. 2; see methods for details). Except for the Amazon and Congo, lateral fluxes and yields are calculated using discharge-weighted means; see Supplementary Information 1c for reference and calculation details.

†GrIS-wide $CH_{4(aq)}$ flux was estimated using the LG discharge-weighted $CH_{4(aq)}$ concentration mean applied to the entire GrIS runoffs; this number is therefore speculative and was included as reference only.

‡From ref. [37]

Areal yields are for entire catchment areas whereas diffusive fluxes refers to stream surface areas.

Extended Data Table 2 | Stable isotope details of CH_4 and CO_2

Sampling Time	$\delta^{13}C$-CH_4 (‰ VPDB)	$\delta^{2}H$-CH_4 (‰ VSMOW)	$\delta^{13}C$-CO_2 (‰ VPDB)
2015-05-04 12:00	-48.9	-	-16.9
2015-05-04 12:00	-46.1	-	-18.4
2015-05-30 11:30	-6.1	-	-12.2
2015-06-07 12:00	-61.3	-303	-15.3
2015-06-07 12:00	-53.1	-281	-16.0
2015-06-17 23:00	-56.7	-313	-15.8
2015-06-17 23:00	-55.2	-256	-14.5
2015-06-21 16:15	-59.3	-235	-22.2
2015-06-21 16:15	-57.6	-289	-24.1
2015-06-25 15:40	-63.4	-308	-14.6
2015-06-25 05:20	-56.6	-302	-14.8
2015-06-26 18:15	-60.2	-272	-23.6
2015-07-01 09:55	-55.9	-318	-26.8
2015-07-01 09:30	-55.2	-262	-26.2

First three rows correspond to borehole and chainsawed-hole collected samples (see Supplementary Information 1b; Extended Data Fig. 3).

Extended Data Table 3 | Site specific parameters applied in the 1D hydrate model

Symbol	Parameter	Value	Unit
z_{xn}	Sediment thickness	20-100	m
h	Ice thickness	1,000	m
G	Geothermal gradient	0.025	°C m^{-1}
T(0)	Basal Temperature	-1	°C
sed	Sedimentation rate	0	m s^{-1}
vup	Upward fluid flux	0	m s^{-1}
φ0	Porosity	0.6	-
R_{xn}	Constant methane production rate	10^{-17} - 10^{-13}	g-CH_4 g^{-1} wet-sediment s^{-1}

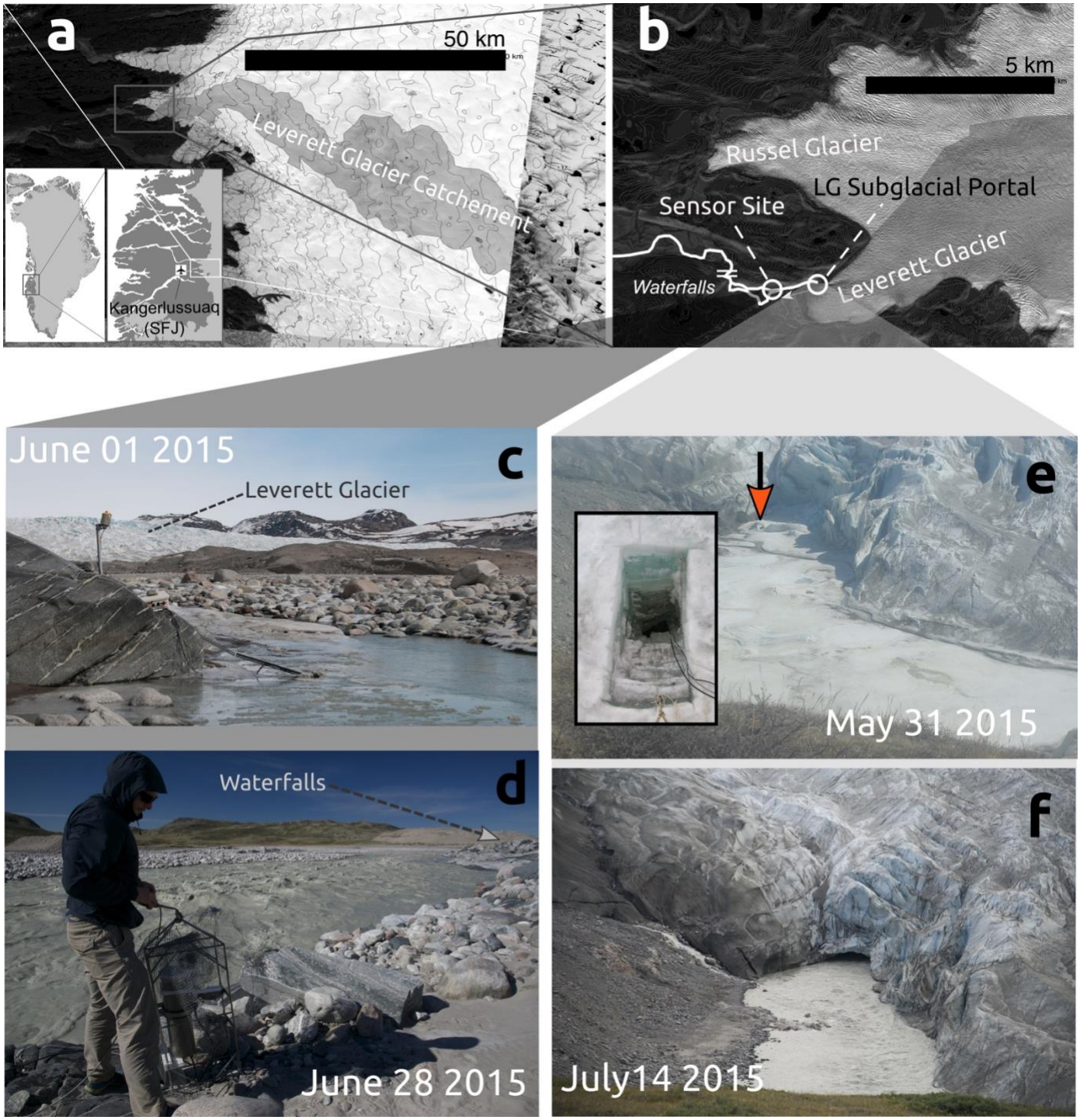

Extended data Fig. 1 | Leverett Glacier and proglacial stream. a Leverett Glacier with catchment boundaries[38] outlined in grey. b Zoomed image of the LG with sampling site and portal marked by dots. c Sensor deployment site during the early melt season with the LG is visible in the background; image faces upstream. d Sensor deployment site in late June; image faces downstream. Also visible is the HydroC® sensor inside steel cage during inspection before re-deployment. e LG portal in late May whilst still covered with both glacial and river ice. Picture was taken an hour before the appearance of the glacial upwelling (see Supplementary Information 2b). Arrow marked the location of the chainsawed hole, visible in the inlet image. Image of the chainsawed hole was taken on May 10 2015. f LG portal in mid-July 2015. Map images courtesy of USGS/NASA Landsat.

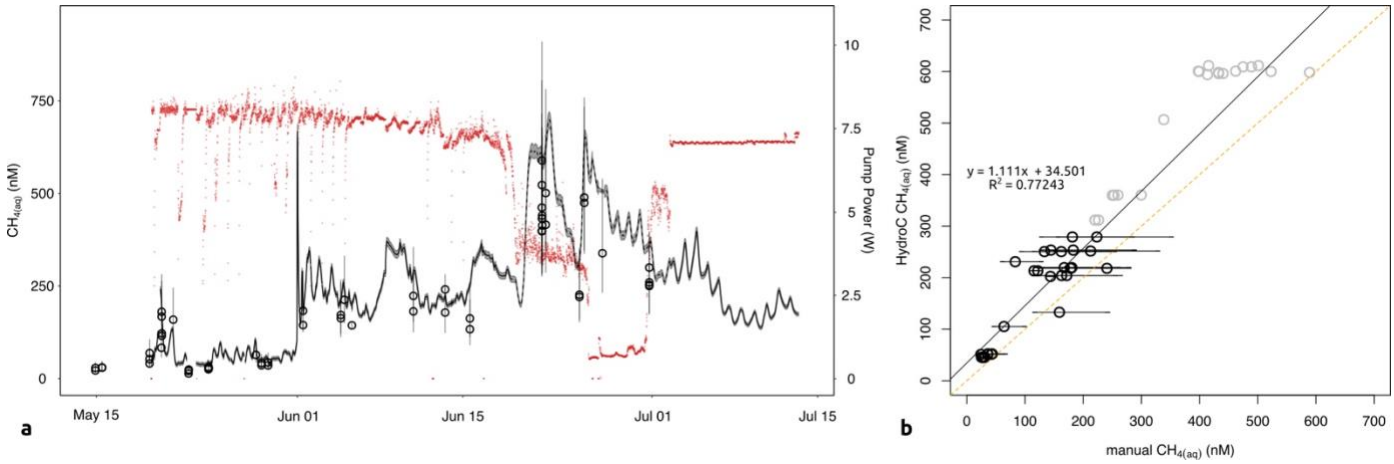

Extended data Fig. 2 | Comparison of CONTROS HydroC® and manual sample $CH_{4(aq)}$ concentrations. a $CH_{4(aq)}$ time-series; red points correspond to the CONTROS HydroC® pump power during operation. Continuous line depicts CONTROS HydroC® measurements with the dashed section corresponding to times when the sensor experienced low pump power and thus a reduced water flow induced by the pump (~ June 19 to July 01); open circles correspond to manual samples. The thin shaded grey area ribbon around the $CH_{4(aq)}$ time-series corresponds to the uncertainty of the CONTROS HydroC® measurements (~ ± 3%); uncertainty on manual measurements indicated through error bars reflects error on vial internal pressures and volumes (119 ± 0.76 mL standard deviation; internal pressures are derived from volumes, see Methods for details). b Regression plot between the CONTROS HydroC® and manual sample measurements. Only manual samples taken during times where CONTROS HydroC® pump power was above ~ 7W were considered for the regression (black circles, black line); grey circles correspond to samples taken during times of lower pump power. Horizontal error bars reflect errors on manual measurements; vertical error bars are smaller than size of circles. Orange line depicts a hypothetical 1:1 relationship between the sensor and manual measurements.

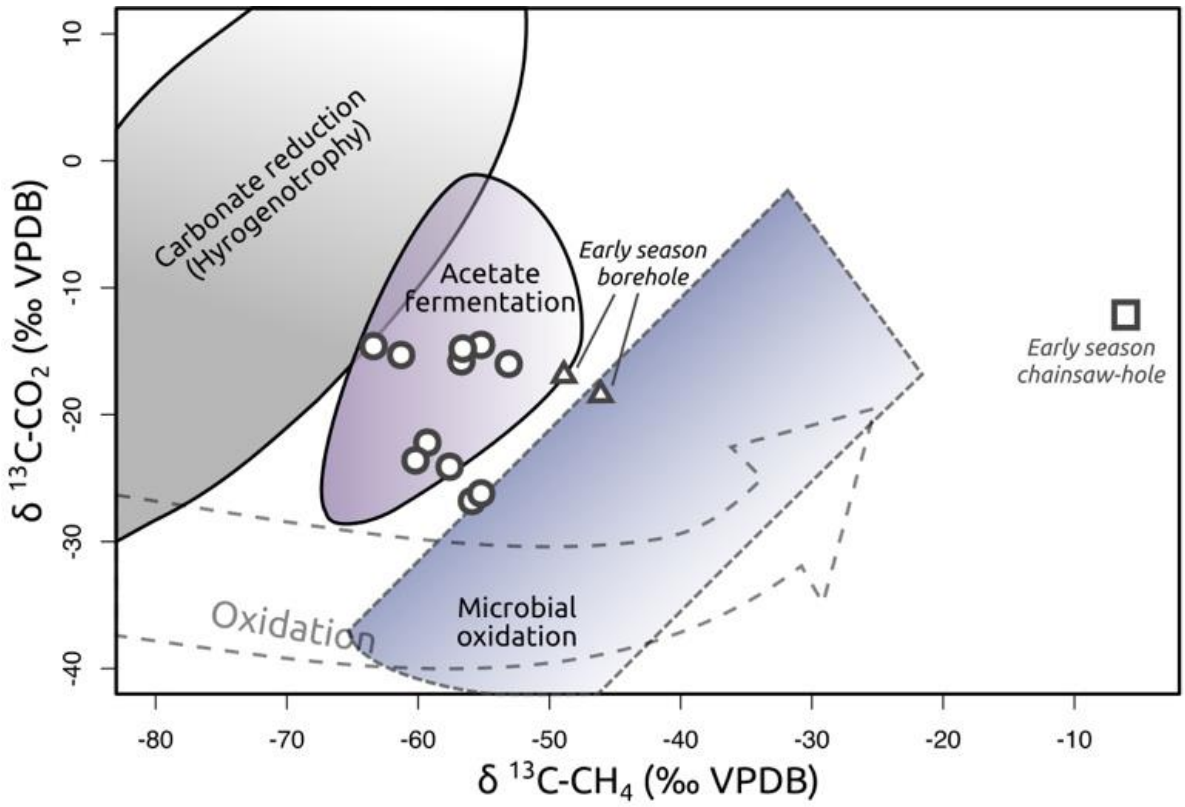

Extended Data Figure 3 | Combination plot of $\delta^{13}C$-CO_2 and $\delta^{13}C$-CH_4 of LG runoff. Points denote $\delta^{13}C$ CO_2-CH_4 values for LG manual samples. Methanogenesis and microbial oxidation classification zones are derived and adapted from ref. [25].

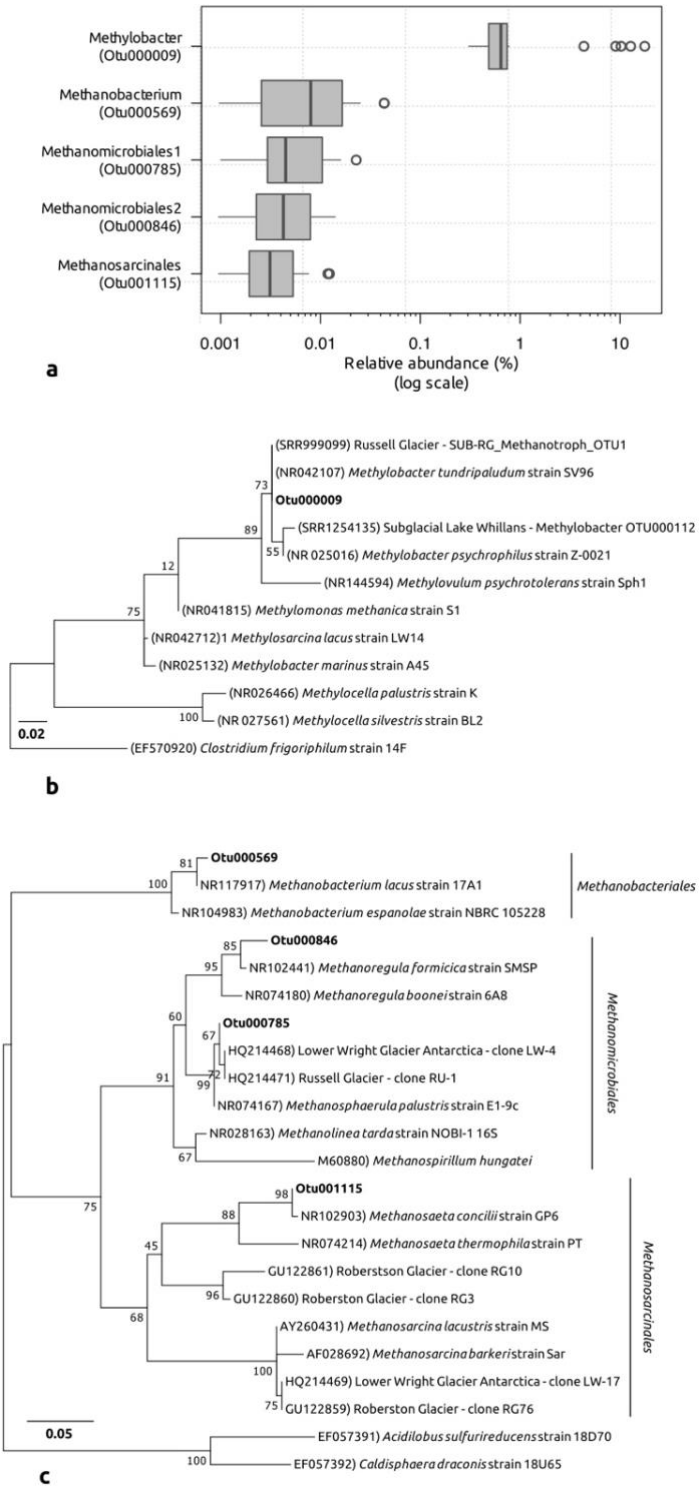

Extended Data Figure 4 | LG 16S rRNA gene sequences related to methanotrophic and methanogenic clades. a Relative abundance of the dominant OTUs related to bacterial methanotrophs (OTU00009) and archaeal methanogens; box mid lines represent medians; the interquartile range (IQR) is represented by the lower and upper box boundaries and denote the 25th and 75th percentiles, respectively; whiskers indicate 1.5 times IQR confidence intervals and points are outliers. b, c Maximum likelihood trees of 16S rRNA sequences related to

methanotrophs rooted with the sequences of *Clostridium frigoriphilum* (b), and methanogens rooted with the sequences of *Acidibilus sulfurireducens* and *Caldisphaera draconis* (c).

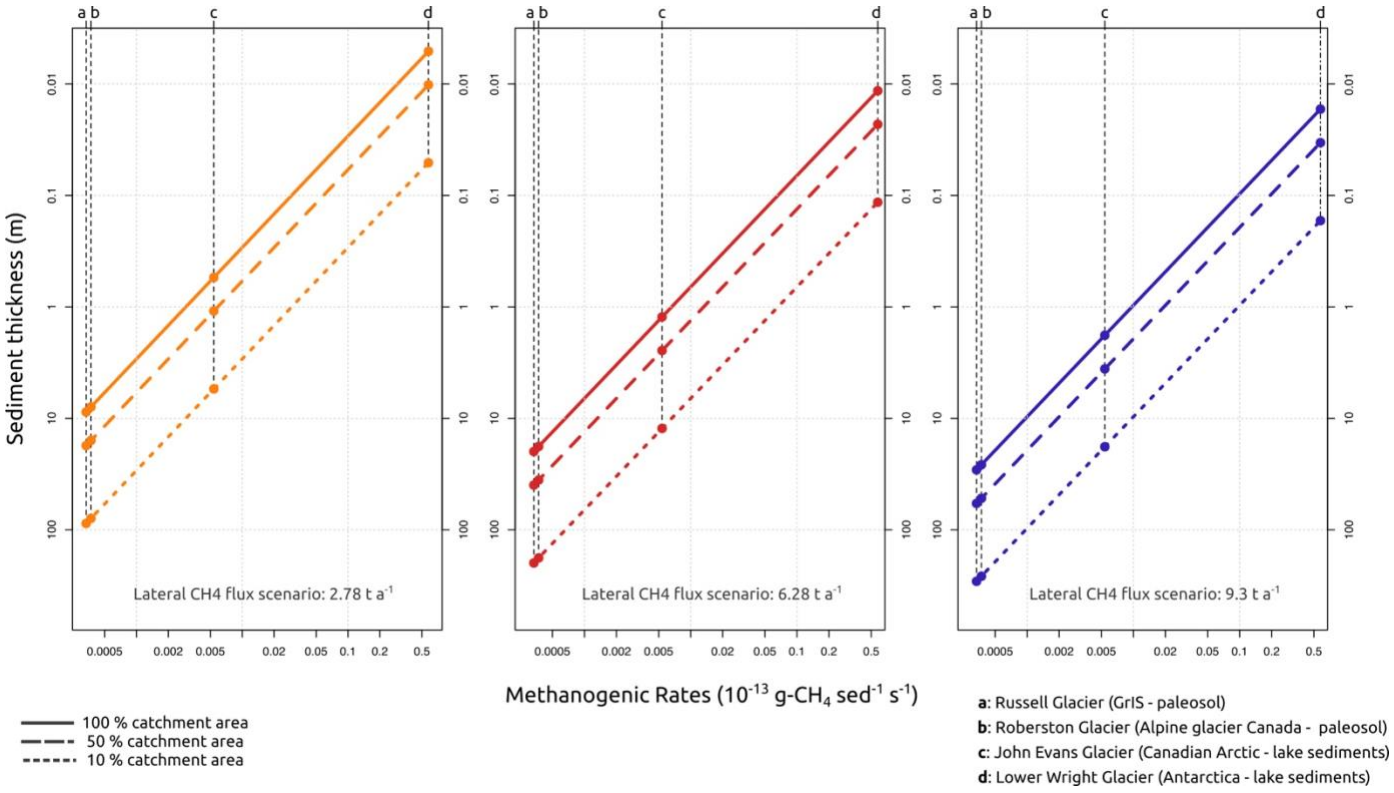

Extended Data Figure 5 | Relationship between rates of subglacial methanogenesis, sediment thickness and observed annual CH_4 flux at LG. Each panel corresponds to the different yearly lateral $CH_{4(aq)}$ flux estimates measured in 2015 (see Fig. 2). Each line type corresponds to the sediment thickness required under different catchment area conditions; whether 100%, 50%, or 10% of the subglacial catchment contribute to the observed CH_4 flux. Any point on a line corresponds to the required methanogenesis rate and subglacial sediment thickness to generate the observed lateral CH_4 flux. The four points on each line correspond to known methanogenic rates recorded from different subglacial habitats[17].

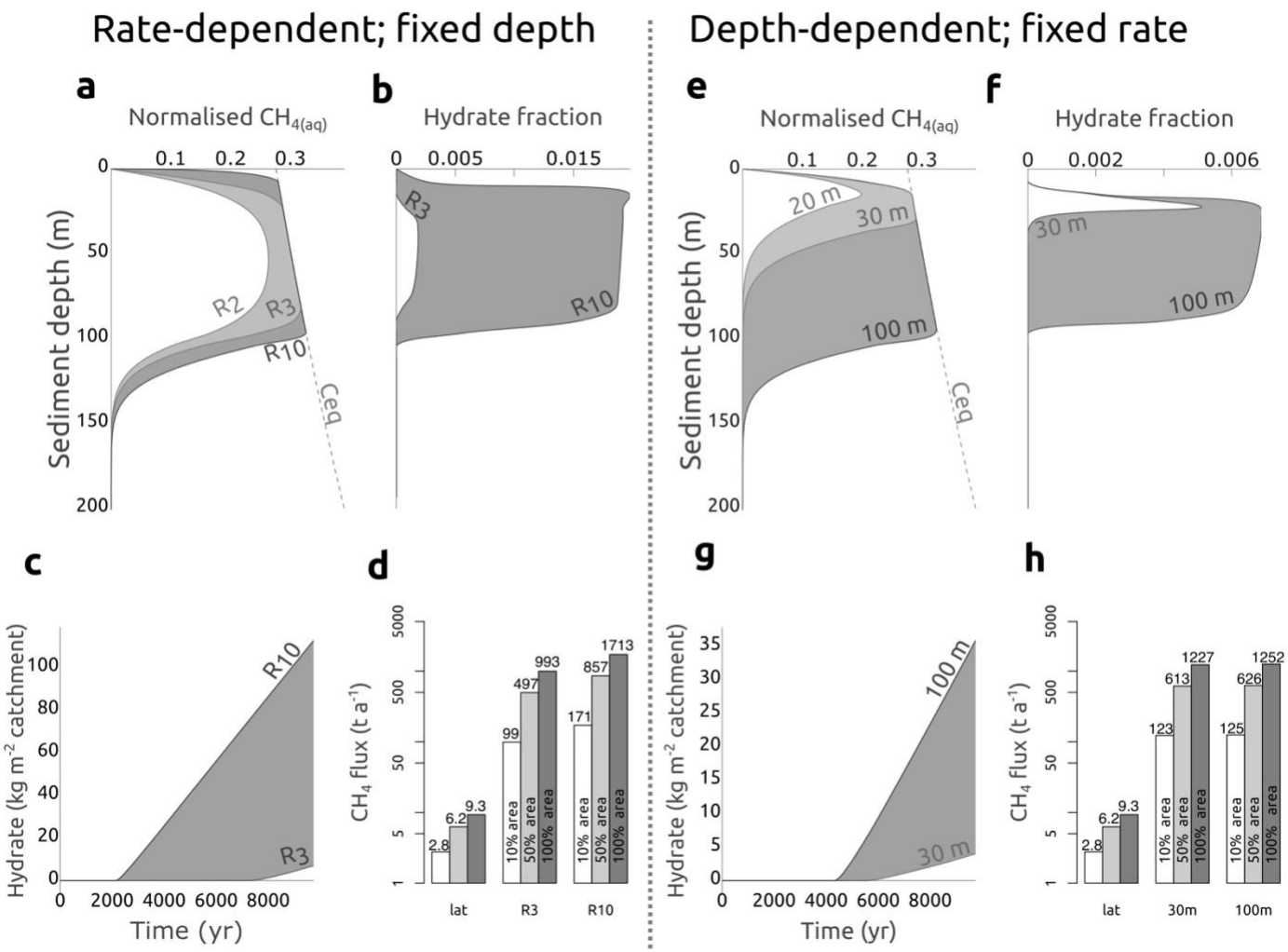

Extended Data Figure 6 | Summary plot of model conditions required for subglacial methane hydrate formation. Left panel indicate model results under a fixed methanogenic depth (100 m) but varying methanogenic rates (R_2 to R_{10}, i.e. 2 to 10^{-15} g-CH_4 g-sediment^{-1} s^{-1}); right panel outputs model runs under a fixed methanogenic rate (5^{-15} g-CH_4 g-sediment^{-1} s^{-1}) but varying methanogenic depths (20-100 m). a, b, e, f: Vertical profiles of methane solubility, dissolved methane, and methane hydrates; methane concentrations are normalised to Ceq (equilibrium concentration). c, g: Time required for methane hydrate formation under modelled conditions. d, h: Diffusive CH_4 flux at the sediment-ice interface under CH_4-hydrate conditions assuming three different catchment CH_4-hydrates cover area (i.e. 10, 50, and 100 % of the LG catchment), compared to the three lateral flux scenarios (a, b, d; Fig. 2) – see supplementary section 2f.

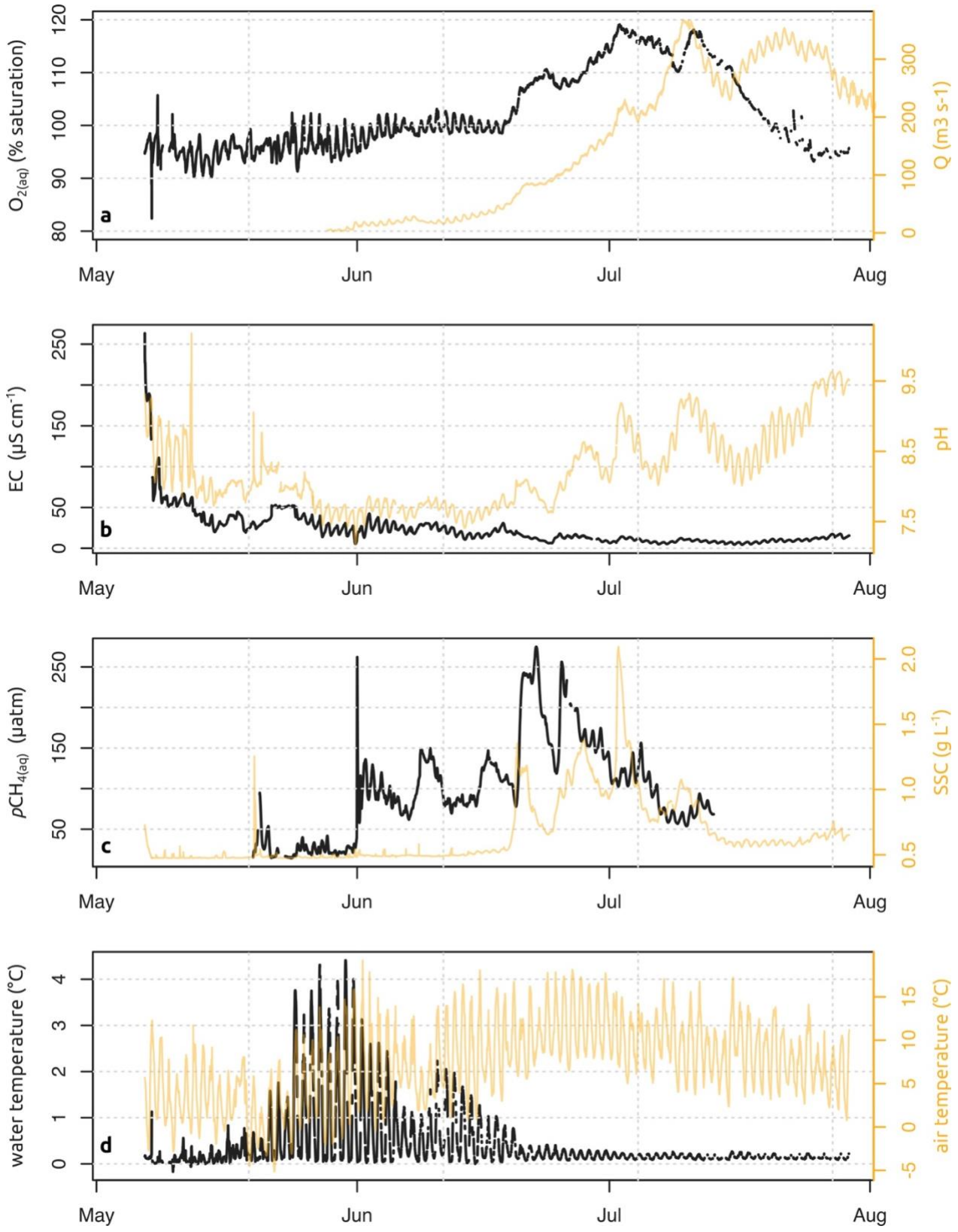

Extended Data Figure 7 | Extended time series of geochemical measurements from the LG proglacial river. EC, pH, and SSC time series include the same as the ones depicted on Fig. 1, but extending to measurements before, and after, the methane record. Note that the $CH_{4(aq)}$ data in c are the CONTROS HydroC® partial pressure (µatm) measurements. Y axes corresponding to black and orange datasets are located on the left and right, respectively.

SUPPLEMENTARY INFORMATION

a. Site Description – Leverett Glacier (LG) catchment hydrology and catchment area

The LG acts as the main outlet to the Russell-Leverett catchment, one of the three large GrIS hydrological basins of the Kangerlussuaq area in South West Greenland[39]. The LG catchment has been the focus of numerous ice-dynamics, hydrology and subglacial biogeochemistry studies in the last decade, and is considered to be highly representative of large areas of Greenland due to its relatively large catchment area, underlying geology (Precambrian orthogneiss and granite) common to much of Greenland[40], and hydrology easily scalable to large regions of the GrIS based on modelled ice sheet runoff and LG discharge (e.g. ref. [15,18,20,30,41-43]). Basal conditions at LG are polythermal, similar to much of the Western margin of the ice sheet which is considered thawed at the bed[44]. The southwestern margin of the GrIS has also experienced the highest degrees of warming in the past decades and is considered the most sensitive ice-sheet region in Greenland to projected temperatures increases in the 21st century, consequently bearing the largest meltwater contribution from the ice sheet[37]; the LG catchment is therefore located in a hydrological "hotspot" of the ice sheet margin.

The LG (surface) catchment covers an area of ~ 1200 km^2 based on surface elevation, extending up to ~ 80 km from the GrIS margin[38]; an area of ~ 600 km^2, however, more accurately depicts the extent of the subglacial catchment[15], with an efficient, fast flowing channelized subglacial system extending to at least 41 km, but less than 57 km, from the ice margin[20]. The relatively large area of the catchment, but, arguably more importantly, the relatively large runoff contribution and very high basal erosion rates at LG makes it of particular interest to understand and evaluate GrIS-wide processes. Overeem et al. (2017)[45] recently surveyed > 160 Greenland outlet glaciers and illustrated that *in situ* measurements of sediment export at LG agreed with satellite and model estimates of Greenland-wide sediment exports to the global ocean. Based on the authors' estimates, the LG catchment ranked 22nd in terms of subglacial catchment area and experienced the 10th largest annual water discharge and 4th highest sediment load of all surveyed catchments.

b. Pre melt-season measurements of ice-margin $CH_{4(aq)}$

In early May, prior to the onset of the melt season, water samples were collected and sensor measurements performed beneath the frozen proglacial river, directly in front of the LG portal

(~20 m downstream of the then-closed subglacial portal; Extended Data Figure 1). Water samples (n=4) were collected on May 2 and 4 through river-ice boreholes (ice thickness ~ 3 m) using the peristaltic pump (see methods). The HydroC CH_4 sensor was also temporally (~24 hours) deployed in a chainsaw-cut hole on May 13. $CH_{4(aq)}$ concentrations in the borehole were ~5.6±0.8 µM and chainsaw hole ~3.5±0.4 µM respectively (mean ± standard deviation).

c. Catchment-normalised areal $CH_{4(aq)}$ yield calculations

In order to allow catchment-wide comparison between methane fluxes observed at LG and other systems, catchment-normalised areal yields of lateral $CH_{4(aq)}$ fluxes were calculated instead of catchment-wide yields from diffusive fluxes normally reported for gaseous species. Lateral fluxes of $CH_{4(aq)}$ most likely account for a larger portion of overall fluxes in glaciated catchments (because most of the catchment is capped by ice) than non-glaciated river basins, where they only amount to a very small fraction of the total fluxes (Extended Data Table 1). Lateral inputs of $CH_{4(aq)}$ feeding proglacial streams are also constrained to a focal source (i.e. ice margin) at the head of the river (as opposed to continuous lateral inputs from smaller-order streams and tributaries to river mainstems), and lateral fluxes from downstream and upstream of the measuring site at LG would be lower and higher, respectively, dependent on methane losses relative to our measuring site.

As opposed to diffusive fluxes, riparian $CH_{4(aq)}$ yields (derived from lateral fluxes) are directly dependent on discharge (and upstream catchment area). LG $CH_{4(aq)}$ concentration measurements were constrained to a single measuring location; consequently, the reported yield is also constrained to the measurement site (methane yields obtained upstream of the measuring sites would be larger and downstream ones smaller, due to $CH_{4(aq)}$ sinks). To more directly compare $CH_{4(aq)}$ yields between LG and other river systems, we focused comparisons to published datasets where both $CH_{4(aq)}$ concentrations and discharge measurements, and ideally drainage-basin area, were available for the same sampling location.

i. Leverett Glacier

The catchment-normalised $CH_{4(aq)}$ yield for the LG site was calculated using the product of the $CH_{4(aq)}$ discharge-weighted mean (i.e. 271 nM) and the total 2015 cumulative discharge (i.e. 1.45 km^3), normalised to the entire glacier catchment (i.e. 600 km^2). Details on estimates of diffusive fluxes at LG are present in the methods section.

ii. Yukon river

Yields for the Yukon river and tributaries were calculated using USGS datasets for specific Yukon-basin gauging stations, which included locations for the Yukon mainstem (i.e. Pilot, Stevens village, and Eagle stations), as well as locations for Yukon tributaries (Koyukuk, Tanana, and Porcupine stations). Except for the Koyukuk station, 2001-2004 $CH_{4(aq)}$ concentration averages were used for calculations[46-49]; the $CH_{4(aq)}$ concentration value for lower-Yukon tributaries in ref. [50] (i.e. 0.77 µM) was used for the Koyukuk station. Discharge-weighted means for each station were used in calculations. Station-specific annual discharge, as well as drainage-basin area, were obtained from the USGS database[51], and a grand average for all available yearly discharge measurements was used in yield calculations. The reported $CH_{4(aq)}$ yields for the Yukon basin were calculated using the grand mean of discharge-weighted concentration means of Koyukuk, Tanana, and Porcupine for the Yukon tributaries, and Pilot, Stevens village, and Eagle for the Yukon mainstem. Diffusive fluxes and associated catchment-wide yields were directly taken from ref. [50].

iii. Lena Delta

Yields obtained for the Lena delta were derived using the overall discharge-weighted mean of the 2009-2010 median $CH_{4(aq)}$ concentrations reported for all three main delta channels (i.e. Trofimovskaya, Bykovskaya, and Olenekskaya channels) in ref. [52]. The complete Lena basin area, as well as the 2002-2012 annual discharge mean (total Lena basin as well as specific channel discharges) were used in calculations[53].

Diffusive fluxes were calculated using the average of the three Lena Delta channel fluxes[52] assigned to the entire surface area of Lena Delta channels. We assumed that the surface area of all river channels within the delta (3,480 km^2) represents 12% of the entire delta area (29,000 km^2) based on ref. [54]. The diffusive flux of the delta was then normalised to the entire Lena river basin area (2,486,000 km^2) in order to obtain a catchment-wide areal yield.

iv. Amazon lower-basin (Negro and Solimões rivers)

The Amazon lower basin yields were calculated using discharge-weighted means of site-specific $CH_{4(aq)}$ concentrations and discharges integrated over a range of water level conditions (i.e. low, high and falling water levels) in 2011-2012[55]. Because drainage area information was not available for each sampling site, discharge-weighted catchment areas of the Negro and Solimões were used when calculating yields of their respective tributaries. In the case of the

Negro, we assigned 290,459 km^2 as the catchment area of its tributaries out of the 686,810 km^2 for the Negro mainstem; 560,747 km^2 of catchment area was assigned to the Solimões tributaries out of the 990,780 km^2 for the mainstem[56]. Diffusive fluxes were directly taken from Table 6 in ref. [55], and associated catchment-wide yields calculated using the mainstem total basin area[56].

v. Congo and Amazon basins

The Congo basin and Amazon-wide basin $CH_{4(aq)}$ yields were calculated using the overall mean of $CH_{4(aq)}$ concentrations reported for the entire Amazon and Congo basins, as well as the basin-wide annual discharge and drainage area[57]. Unlike the previous sites, the calculated yields only represent gross estimates because no information on sampling-site discharge and drainage-basin area was available. Diffusive fluxes and associated yields for the Amazon- and Congo-wide basins were obtained from ref. [58] and [59] respectively. In the case of the Congo, the average of the fluxes reported using the "Auf" and "Ray" methods was used (see ref. [59]).

d. Molecular analyses of LG runoff

Between ~ 600 – 2000 mL of LG bulk runoff was filtered through Sterivex filters (Millipore, USA) between May 04 and July 26 (n = 31). Sterivex filters were preserved in MoBio RNA LifeGuard solution (MoBio Laboratories, USA) immediately after sampling, frozen inside portable freezer within 1 hour of collection. DNA was extracted using the DNeasy PowerWater Sterivex kit (MoBio Laboratories, USA) following the manufacturer's protocol. Extracted DNA samples were sequenced at the Mr. DNA Molecular Research facility (Shallowater, TX, USA; http://www.mrdnalab.com/) on an Illumina MiSeq platform using the 515f/806r primer pair, which targets the 16S rRNA V4 hypervariable region[60].

Sequences were analysed on the mothur platform v.1.38.1[61] following the mothur MiSeq standard operation procedure[62]. Sequences were binned into operational taxonomical units (OTU) at a 97% sequence identity level and classified against the SILVA (v.123) database. Maximum likelihood phylogenetic trees containing the representative sequence of the dominant OTUs related to methanotrophic and methanogenic sequences were assembled in MEGA v.7.0.26.

2. Supplementary Discussion

a. Manual samples and CONTROS HydroC response time

$CH_{4(aq)}$ concentrations obtained by manual samples generally agreed with HydroC results for most of the measuring period when the sensor's pump power was maintained over ~ 7W; the large error on manual measurements relates to uncertainties of internal vial pressures (i.e. 3.5 ± 0.9 atm) (Extended Data Fig. 2). The small deviation between HydroC and manual sample measurements (Extended Data Fig. 2.b) may also relate to the presence of air bubbles during manual sampling. Whilst care was taken to exclude any air bubble during sampling, we cannot exclude the possibility that a small amount of air bubbles may have been present in some samples due to the highly turbulent waters during sampling. Air contamination in manual samples would result in a slight underestimation of methane concentrations.

The repetitive drops in pump power during the first parts of the measurement period (May 19 – June 19, Extended Data Fig. 2) correspond to the changes in power sources (i.e. solar-charged battery versus back-up generator) to the sensor that were necessary during evenings and mornings. Only solar-charged batteries were used after June 19 (due to increased solar irradiance), reflected by the more stable power output (Extended Data Fig. 2). A drop in power to the HydroC pump (SBE-5T) between June 19 – 30, however, most likely affected the HydroC response time and measurements during that period may not have accurately captured changes in $CH_{4(aq)}$ concentrations as reflected by a more pronounced difference between manual samples and sensor measurements. The high degree of uncertainty associated with manual measurements, however, limits their use as exact reference points during that period (Extended Data Fig. 2). Inefficient pumping of water to the HydroC can affect the CH_4 equilibration time between the membrane and the detector chamber of the sensor, causing measurement lags.

This drop in pump power was most likely caused by the rapid increases in suspended particulate matter levels during the first two outbursts (Fig. 1), which may have impeded the movement of the magnetically coupled impeller (pump power is proportional to pump rate). Despite a probable slower measurement response from the sensor during times of lower pump power, sharp peaks and troughs in $CH_{4(aq)}$ levels were still captured by the sensor during that period, reflective of outburst events and discrete subglacial methane flushing, as well as diurnal patterns (Fig. 1). Because the overall changes in $CH_{4(aq)}$ mimicked changes in SSC, E.C., and

pH, we consider them to approximately depict evolution of $CH_{4(aq)}$ concentrations, even if the magnitude of those exports may be under-represented. Correcting for HydroC measurement lags[63,64] are unlikely to change the overall $CH_{4(aq)}$ concentration trend observed here with respect to outburst events and diurnal cycles, which happen on the timescale of several hours to days (the HydroC response time, t_{63}, under optimal conditions at 2-3°C water temperature is < 30 minutes).

b. Evolution of the LG subglacial drainage system and concomitant methane export behaviour

The LG hydrological system displays features which are reported in many glaciers worldwide, and likely is typical of GrIS catchments more generally. Surface meltwaters are routed to the bed via supraglacial openings (e.g. crevasses and moulins) caused by fracturing of the ice, connecting sub- and supraglacial environments. The subglacial drainage system consequently undergoes a seasonal evolution following the upglacier progression of the snowline driven by the increase in surface runoff entering the subglacial environment[20,65-67]. It evolves from a slow, inefficient hydrological system with tortuous flow pathways early in the melt season, to a rapidly draining efficient system[20]. At LG, subglacial runoff ultimately exits the catchment via a well-defined portal that feeds its proglacial river (Extended Data Fig. 1).

Early melt-season (prior to June 19 2015)

During early sensor deployment, most of the proglacial river was still ice-covered, with waters at the measuring site largely derived from a mixture river-ice meltwaters and marginal runoff (Extended Data Fig. 1). The very high EC and pH values recorded during that period, however, also indicate a significant contribution from basal meltwaters (Fig. 1). Elevated EC and high pH are indeed typical of subglacial environments, and the geochemistry of the LG proglacial river prior to major melt events in the season is mostly influenced by slow inefficient marginal basal meltwaters from the distributed subglacial system[18]. Because of the very small discharge in the early melt season, even a small contribution from subglacial waters has an important influence on the hydrochemistry profile of the proglacial river.

Methane concentrations during this period were the lowest recorded (mean ~55 nM) but were significantly higher than background-equilibration concentrations (~4 nM at local water temperatures). The abrupt pulse in methane on May 31-June 01 coincided with the opening of

the subglacial conduit at LG, marked by the appearance of a water upwelling through river ice in front of the then ice-sealed LG portal, and resulting in a relative increase in discharge indicative of larger influences from meltwaters (Fig. 1). The dramatic increase in methane concentrations and sustained high EC during and following the appearance of the subglacial upwelling most likely reflects the release of over-winter stored subglacial waters enriched in methane from the ice margin (see Supplementary Information 1b). Similarly, the two methane peaks recorded on June 8 and 15 likely represent the connection of proximal distributed system waters, also consistent with rises in EC during those two events (Fig. 1).

Outburst period (June 19 to July 13 2015)

Export of long-residence-time subglacial waters from the glacier bed is accentuated during increases in the rate of supraglacial meltwater delivery into the subglacial drainage system, often producing distinct pulses of enhanced water runoff superimposed on the general pattern of runoff growth[18]. Large pulses of meltwater alter the basal water pressure and enable the expansion of efficient subglacial drainage pathways into previously inefficient areas of the ice sheet bed[68,69]. The precise timing of distinct runoff pulses is generally associated with sudden catastrophic drainage of meltwater stored in supraglacial lakes which force a surface-to-bed drainage connection through hydro-fracture, or routing of large volumes of meltwater to the ice-sheet bed via englacial conduits such as crevasses and moulins[18,69]. Periods of subglacial water release via outbursts are typically accompanied by peaks in electrical conductivity (EC) and suspended sediment, reflecting the evacuation of sediments and solute-rich water from basal environments; pH spikes (Fig. 1) are also consistent with increased mobilisation of long residence time subglacial waters which have undergone substantial chemical weathering[70]. Herein, we refer to such events as outbursts.

The first outburst on June 19 marked a pronounced increase in meltwater discharge, and the growth of an efficient subglacial drainage system at LG, allowing the rapid evacuation of meltwaters to the ice margin. From this point forward, and during the rest of the observation period, the subglacial drainage system at LG undergoes a rapid upglacier expansion[20]. A series of supraglacially forced outburst events are normally observed at LG during this expansion period where new regions of the bed become accessible and connected to efficient drainage channels[18]; in 2015 these events occurred broadly coincidently with the step-wise retreat of the snowline to higher elevations, increasing the supraglacial catchment area[16].

The four methane concentration pulses that accompanied the recorded four outburst events during the observation period indicate that newly connected methane-bearing regions of the bed act to sustain methane fluxes beyond the early melt period (Fig. 1). It also illustrates that sediment-rich, long-residence-time waters from the distributed drainage system contain high concentrations of methane, which can be rapidly exported to the ice-margin once connected to efficiently-draining channels.

Supraglacially forced pulses in methane concentrations appear to lag those of other geochemical parameters (EC, pH, and SSC; Fig. 1). We attribute this lag to a momentary dilution of methane-rich subglacial waters by the sudden input of high volumes of low-methane-concentration supraglacial runoff waters, illustrated by abrupt, but brief, drops in methane concentrations at the onset of the recorded outburst events, where the latter caused increased subglacial pressures. The subsequent abrupt rises in methane levels (most evident during the first two outbursts; Fig. 1) can be explained by mobilisation of methane rich distributed system water, associated with the water pressure decrease that likely followed the rapid evacuation of supraglacial lake waters in a newly expanded channelized system. This promoted the flow of distributed water sources along the pressure gradient towards the main subglacial channel[67,70].

This behaviour is most evident during the first two recorded outbursts, most likely due to a closer proximity to the ice margin and lower discharge, which translate into a more pronounced effect on the methane concentration graph (Fig. 1). The effects of these localised events on methane concentrations later in the melt season (outbursts 3 and 4) are indeed dwarfed by a larger meltwater contribution from a more developed channelized drainage system, reflected by the absence of sharp methane pulses following the onset of the two later outbursts, as well as the persistence of a strong diurnal pattern observed during the rising limb of the methane-concentration peaks (Fig. 1). Because the overall methane load remained high during those later outbursts (Fig. 1), the absence of sharp methane concentration peaks is likely caused by the continuous dilution from ice melt generated from a larger overall catchment area.

Outburst occurrences at LG are normally limited to the first half of the ablation season, when supraglacial lakes and melt ponds drain and drive rapid expansion of the efficient subglacial drainage system[15,18]. The evolution of an efficient subglacial hydrological system at LG

progresses to ~ 41 km upglacier after reaching a cumulative discharge of ~ 0.78 km^3 based on SF_6 injection tracer experiments[20] (in 2015 a cumulative discharge of 0.78 km3 was reached on July 26). Once fully established, sustained fluxes of solute and suspended sediments in runoff indicate a continued flow contribution by distributed system waters during the rest of the season (i.e. SSC and ions; e.g. ref. [15,18,30]). The continuous methane record ended on July 13; the sustained load of methane observed during the end of the measuring period did not indicate any sign of exhaustion of subglacial methane reserves (Fig. 1). Like other chemical species (major ions, dissolved organic carbon[71]), we hypothesize that methane export during the second period of the melt season will follow similar behaviour to SSC (Extended Data Fig. 7c).

c. Inferred methanotrophy in LG runoff

Methanotrophic rates at LG were not directly measured. However, non-poisoned water samples (without $HgCl_2$ to inhibit microbial activity) revealed a decrease in methane concentrations up to 100-fold relative to microbially fixed samples upon analyses back in the home laboratory (data not shown), indicating that active methanotrophs were present at the site. Moreover, a strong microbial oxidation isotopic signature[25] characterised the borehole and chainsaw hole manual samples collected through river ice in front of the LG prior to the onset of the melt season. We attribute the stronger methanotrophic effect (enrichment in heavy stable isotope) of the samples collected in the chainsawed open-hole versus the borehole-collected waters to the likely higher oxygen concentrations present in the surface waters of the chainsaw hole, which had been exposed to the atmosphere for 20 days prior to sampling (Extended Fig. 3).

To estimate the impact of aerobic microbial oxidation upon methane concentrations in subglacial channels *en route* to the glacier terminus, we used a previously measured methanotrophic rate from proglacial stream samples of the neighbouring Russell Glacier (RG)[5]. RG is part of the same overall ice-sheet catchment as the LG, overlaying same geological settings; environmental factors impacting microbial oxidation at LG should therefore be similar to the ones present at RG. Moreover, molecular analyses of the LG river revealed that the dominant methanotrophic clade sampled had identical (100% identity) partial 16S rRNA-gene sequences to the one identified at RG (Extended Data Fig. 4b).

We therefore consider that the use of the Dieser et al. 2014 reported microbial rate to be representative of the methanotrophic sink at LG. In fact, the RG oxidation rate likely exceeded

in situ methanotrophy at LG for most our measuring period, given the higher temperature (i.e. 4°C) and higher methane concentrations in meltwaters employed in the Dieser et al. 2014 incubations. The lower LG river temperatures (Extended Data Fig. 7d), as well as lower overall methane concentrations (i.e. lower substrate availability), should result in overall lower methanotrophic rates[72,73]. Additionally, a smaller methanotrophic footprint at LG relative to RG is consistent with the lower relative abundance of 16S rRNA gene sequences related to methanotrophic clades detected in the LG runoff (~ 0.5 to 10 % of total OTUs at LG (Extended Data Fig. 4.a)) than at RG (~ 1 – 60 %)[5]. As such, we consider the use of the Dieser et al. (2014) microbial oxidation rate to be conservative and likely represent higher limits.

A small methanotrophic impact on subglacial methane during its transit through the glacier drainage system is also consistent with the ^{2}H- and ^{13}C-CH_4 isotopic signature of samples collected later in the season, at a time of higher flow and thus, short residence times (see methods). Conversely, water samples collected earlier in the season show more oxidised signatures (Extended Data Fig. 3) which is consistent with their source from mostly stagnant waters beneath the river ice in front of the LG, where methane production and oxidation would be expected to be in a near equilibrium state.

A similar methanotrophic effect to these latter stagnant or more slowly flowing meltwaters was also observed in the Antarctic Subglacial Lake Whillans, where microbial oxidation was found to strongly impact the concentrations and isotopic signature of methane diffusing from the underlying lake sediments[3]. We therefore suggest that microbial oxidation may have a strong buffering effect on subglacial methane fluxes in steady-state systems (e.g. stagnant subglacial lake waters or in systems dominated by passive, diffusive fluxes), but that the microbial sink observed under such stable conditions may have a much smaller buffering impact during rapid subglacial drainage events, such as the ones observed here in Greenland, which completely alter the nature of the putative methanotrophic layer.

d. LG methanogen populations and subglacial methanogenic substrates

Overall, archaeal sequences constituted a minority of the recovered microbial diversity of the LG proglacial stream, amounting to less than 1% of the total microbial classified OTUs. Focusing on archaeal diversity alone, however, identified the presence of archaeal sequences related to both hydrogenotrophic and acetoclastic clades of methanogens amongst the most abundant archaeal OTUs (here defined to OTUs amounting to >1% archaeal relative

abundance). Interestingly, whereas methane stable isotopes pointed to a dominance of acetate-derived methane generated from the LG catchment (Fig. 4; Extended Data Fig. 3), three of the four most abundant methanogen-related OTUs from the LG stream most closely matched sequences from hydrogenotrophic methanogens (i.e. related to *Methanobacteriales* and *Methanomicrobiales* strains; Extended Data Fig. 4). It is important to point out that 16S rRNA gene data alone cannot infer microbial activity. The low relative abundance of the methanogen-related OTUs (<0.1% of overall 16S rRNA gene library) further limits the use of molecular data to conclude on the relative contribution of each methanogen clade towards the overall LG methane pool and original methanogenic substrate (H_2 or acetate) utilised by subglacial methanogen populations beneath the catchment.

Acetate-derived methane beneath the LG is consistent with findings of CH_4 originating from relatively old OC from recently deglaciated marginal lakes in the Kangerlussuaq area[23] (Fig. 4). The lighter CH_4 stable isotopic signature found in these lakes compared to the LG CH_4 (Fig. 4) could partially result from substrate maturation[25], where methane from the LG catchment would be generated from older source material. Recent ^{14}C analyses of particulate organic carbon at LG indeed demonstrated average radiocarbon ages of > 4,000 years[16], compared to CH_4 bearing a ^{14}C signature of 1,400 – 1,500 years for Greenland marginal lakes[23]. The likely contribution to methane production from multiple pathways at LG is suggestive of a progressive transition from organic (e.g. acetate) to inorganic (H_2/CO_2) methane substrates (e.g. derived from bedrock comminution[24]) reflecting a depletion of the labile organic carbon pool in further inland regions, overlaid by the ice sheet for longer time periods. This putative "inorganic switch" is consistent with GISP2 and GRIP ice core, as well as Subglacial Lake Whillans sediment data, which all identified subglacial methane to be derived from H_2 oxidation/CO_2 reduction, as indicated by stable isotopes[8,12,74] (Fig. 4).

e. Subglacial methanogenic rates and sediment thickness

The methanogenic rates required to sustain the observed methane flux at LG are dependent on the subglacial habitat present beneath the ice. No consensus exists regarding the state of the bed beneath the GrIS. Studies at LG often assumed a hard bed directly underlying the ice (e.g. in ref. [15]), whilst others have alluded to at least meters-thick subglacial sediments for a neighbouring catchment[75], as well as sediment layers potentially hundreds of meters thick in other regions of the GrIS[27]. Orders of magnitude also separate methanogenic rates measured from different subglacial environments, with rates from lacustrine- or marine-derived

subglacial sediments from Antarctic glaciers much higher than those reported for Greenland and alpine glaciers overlaying paleosol[17].

Extended Data Fig. 5 describes the relationship between subglacial methanogenic rates and sediment thickness required to sustain the observed methane cumulative exports recorded in 2015. Interestingly, if methanogenic rates observed for Greenland basal ice sediments apply to the LG catchment, at least ~ 9 - 29 m of sediment across the catchment are required for subglacial methanogenic populations to match the annual $CH_{4(aq)}$ flux recorded in 2015 (Extended Data Fig. 5). It should be noted that these estimates represent a lower limit on both methanogenic rates and sediment thickness needed to exactly match 2015 methane export, under a scenario where the entire catchment is warm-based with a uniform sediment layer, and where subglacial methane production exactly matches annual methane discharges, ignoring (residual) methane build-up beneath the catchment. The possibility for residual methane to build-up under LG, potentially leading to methane hydrate formation is discussed below. Would only a subsection of the LG catchment contribute to methane export (likely), then thicker sedimentary pockets would be required to account for the observed methane flux (Extended Data Fig. 5). Recent seismic evidence from the Russell-Leverett catchment suggests the presence of a sedimentary layer beneath the ice[76]. However, ice flow observations and models, as well as borehole investigations from Western Greenland indicate that if thick sedimentary layers do exist beneath the ice, they likely are patchily distributed[77,78].

f. Subglacial CH_4-hydrate evolution

A 1D reaction-transport model was used to assess the plausibility of methane hydrate accumulation in the LG catchment. For this purpose, the model was applied to quantify the magnitude of methane production rates that would be required to accumulate CH_4-hydrates under plausible, but optimal environmental conditions in the LG catchment. Methane hydrates form in the sediment when constant methane production rates exceed the diffusive methane loss through the sediment-ice interface and allow for the accumulation of methane in porewaters beyond the saturation concentration. Simulation results indicated that several tens of meters of sediments, and at least several thousand years are required in order to form and maintain CH_4-hydrate reservoirs at LG (Extended Data Fig. 6). Assuming a 100 m thick methanogenic-sediment layer, a methane production rate of ~ 3×10^{-15} g-CH_4 g^{-1} sediment s^{-1} (about two orders of magnitude higher than that observed in GrIS basal ice incubations[17],

Extended Data Fig. 5) is required to form CH_4-hydrates after just under 8,000 years of sustained methane production (Extended Data Fig. 6 a, b, c). Thinner sediments would require higher methane production rates; e.g. at least 30 m thick sediments are needed to form CH_4-hydrates assuming a sustained methanogenic rate of 5×10^{-15} g-CH_4 g^{-1} sediment s^{-1} (Extended Data Fig. 6 e, f).

Because CH_4-hydrate formation requires oversaturation of porewaters, model scenarios that result in the formation of methane hydrates in the LG catchment are associated with high dissolved methane concentrations (close to the methane-hydrate equilibrium line) in shallow sediments and, thus, large concentration gradients at the sediment-ice interface. As a consequence, the catchment wide diffusive methane fluxes through the sediment-ice interface generated under such CH_4-hydrate-stable conditions would result in hundreds of t-CH_4 a^{-1}, over an order of magnitude larger than the observed lateral fluxes at LG (i.e. 2.5-9.3 t-CH_4 a^{-1}; Extended Data Fig. 6 d, h). These estimates, however, depend on the overall catchment area bearing CH_4-hydrates (Extended Data Fig. 6 d, h). Considering the likely patchiness of sedimentary layers beneath the ice sheet (see above section), it may be possible that distributed, deep sediment sections do exist beneath the LG catchment that could favour methane hydrate evolution and potentially account for some of the methane flux observed at LG. Given our current estimations of overall methane export from the catchment, however, it seems unrealistic that the bulk of methane measured at LG originates from CH_4-hydrate-bearing sediments. That being said, the required conditions to form CH_4-hydrate layers beneath 1,000 m of ice are not unrealistic for other regions of the GrIS, where thick ice cover has been present for long time periods (>10,000 years) and where thick sedimentary layers are also likely present (e.g. ref. [27]).

References

1 Kirschke, S. *et al.* Three decades of global methane sources and sinks. *Nature Geosci* 6, 813-823, doi:10.1038/ngeo1955 (2013).

2 Schaefer, H. *et al.* A 21st century shift from fossil-fuel to biogenic methane emissions indicated by 13CH4. *Science* (2016).

3 Wadham, J. L., Tranter, M., Tulaczyk, S. & Sharp, M. Subglacial methanogenesis: A potential climatic amplifier? *Global Biogeochem. Cycles* **22**, n/a-n/a, doi:10.1029/2007gb002951 (2008).

4 Wadham, J. L. *et al.* Potential methane reservoirs beneath Antarctica. *Nature* **488**, 633-637, doi:10.1038/nature11374 (2012).

5 Dieser, M. *et al.* Molecular and biogeochemical evidence for methane cycling beneath the western margin of the Greenland Ice Sheet. *ISME J* **8**, 2305-2316, doi:10.1038/ismej.2014.59 (2014).

6 Stanley, E. H. *et al.* The ecology of methane in streams and rivers: patterns, controls, and global significance. *Ecological Monographs* **86**, 146-171, doi:10.1890/15-1027 (2016).

7 Weitemeyer, K. A. & Buffett, B. A. Accumulation and release of methane from clathrates below the Laurentide and Cordilleran ice sheets. *Global and Planetary Change* **53**, 176-187, doi:10.1016/j.gloplacha.2006.03.014 (2006).

8 Michaud, A. B. *et al.* Microbial oxidation as a methane sink beneath the West Antarctic Ice Sheet. *Nature Geosci* **10**, 582-586, doi:10.1038/ngeo2992 (2017).

9 Petrenko, V. V. *et al.* Minimal geological methane emissions during the Younger Dryas–Preboreal abrupt warming event. *Nature* **548**, 443-446, doi:10.1038/nature23316 (2017).

10 Portnov, A., Vadakkepuliyambatta, S., Mienert, J. & Hubbard, A. Ice-sheet-driven methane storage and release in the Arctic. *Nat Commun* **7**, doi:10.1038/ncomms10314 (2016).

11 Souchez, R., Lemmens, M. & Chappellaz, J. Flow-induced mixing in the GRIP basal ice deduced from the CO2 and CH4 records. *Geophysical Research Letters* **22**, 41-44, doi:10.1029/94GL02863 (1995).

12 Miteva, V., Teacher, C., Sowers, T. & Brenchley, J. Comparison of the microbial diversity at different depths of the GISP2 Greenland ice core in relationship to deposition

climates. *Environmental Microbiology* **11**, 640-656, doi:10.1111/j.1462-2920.2008.01835.x (2009).

13 Christner, B. C., Montross, G. G. & Priscu, J. C. Dissolved gases in frozen basal water from the NGRIP borehole: implications for biogeochemical processes beneath the Greenland Ice Sheet. *Polar Biol* **35**, 1735-1741, doi:10.1007/s00300-012-1198-z (2012).

14 Schmidt, M., Linke, P. & Esser, D. Recent Development in IR Sensor Technology for Monitoring Subsea Methane Discharge. *Marine Technology Society Journal* **47**, 27-36, doi:10.4031/MTSJ.47.3.8 (2013).

15 Cowton, T., Nienow, P., Bartholomew, I., Sole, A. & Mair, D. Rapid erosion beneath the Greenland ice sheet. *Geology* **40**, 343-346 (2012).

16 Kohler, T. J. *et al.* Carbon dating reveals a seasonal progression in the source of particulate organic carbon exported from the Greenland Ice Sheet. *Geophysical Research Letters*, 6209-6217, doi:10.1002/2017GL073219 (2017).

17 Stibal, M. *et al.* Methanogenic potential of Arctic and Antarctic subglacial environments with contrasting organic carbon sources. *Global Change Biology* **18**, 3332-3345, doi:10.1111/j.1365-2486.2012.02763.x (2012).

18 Bartholomew, I. *et al.* Supraglacial forcing of subglacial drainage in the ablation zone of the Greenland ice sheet. *Geophysical Research Letters* **38**, n/a-n/a, doi:10.1029/2011GL047063 (2011).

19 Raymond, P. A. *et al.* Global carbon dioxide emissions from inland waters. *Nature* **503**, 355-359, doi:10.1038/nature12760 (2013).

20 Chandler, D. M. *et al.* Evolution of the subglacial drainage system beneath the Greenland Ice Sheet revealed by tracers. *Nature Geosci* **6**, 195-198, doi:10.1038/ngeo1737 (2013).

21 Hall, R. O., Kennedy, T. A. & Rosi-Marshall, E. J. Air–water oxygen exchange in a large whitewater river. *Limnology and Oceanography: Fluids and Environments* **2**, 1-11, doi:10.1215/21573689-1572535 (2012).

22 Maurice, L., Rawlins, B. G., Farr, G., Bell, R. & Gooddy, D. C. The Influence of Flow and Bed Slope on Gas Transfer in Steep Streams and Their Implications for Evasion of CO2. *Journal of Geophysical Research: Biogeosciences* **122**, 2862-2875, doi:10.1002/2017JG004045 (2017).

23 Walter Anthony, K. M., Anthony, P., Grosse, G. & Chanton, J. Geologic methane seeps along boundaries of Arctic permafrost thaw and melting glaciers. *Nature Geosci* **5**, 419-426 (2012).

24 Telling, J. *et al.* Rock comminution as a source of hydrogen for subglacial ecosystems. *Nature Geosci* **8**, 851-855, doi:10.1038/ngeo2533 (2015).

25 Whiticar, M. J. Carbon and hydrogen isotope systematics of bacterial formation and oxidation of methane. *Chemical Geology* **161**, 291-314, doi:10.1016/S0009-2541(99)00092-3 (1999).

26 Etiope, G. & Sherwood Lollar, B. Abiotic methane on Earth. *Rev. Geophys.* **51**, 276-299, doi:10.1002/rog.20011 (2013).

27 Walter, F., Chaput, J. & Lüthi, M. P. Thick sediments beneath Greenland's ablation zone and their potential role in future ice sheet dynamics. *Geology* **42**, 487-490 (2014).

28 Wingham, D. J., Siegert, M. J., Shepherd, A. & Muir, A. S. Rapid discharge connects Antarctic subglacial lakes. *Nature* **440**, 1033-1036, doi:10.1038/nature04660 (2006).

29 Beaton, A. D. *et al.* High-Resolution in Situ Measurement of Nitrate in Runoff from the Greenland Ice Sheet. *Environmental Science & Technology* **51**, 12518-12527, doi:10.1021/acs.est.7b03121 (2017).

30 Hawkings, J. R. *et al.* Ice sheets as a significant source of highly reactive nanoparticulate iron to the oceans. *Nat Commun* **5**, 3929, doi:10.1038/ncomms4929 (2014).

31 Ward, J. A. *et al.* Microbial hydrocarbon gases in the Witwatersrand Basin, South Africa: Implications for the deep biosphere. *Geochimica et Cosmochimica Acta* **68**, 3239-3250, doi:10.1016/j.gca.2004.02.020 (2004).

32 Wiesenburg, D. A. & Guinasso Jr, N. L. Equilibrium solubilities of methane, carbon monoxide, and hydrogen in water and sea water. *Journal of Chemical and Engineering Data* **24**, 356-360 (1979).

33 Raymond, P. A. *et al.* Scaling the gas transfer velocity and hydraulic geometry in streams and small rivers. *Limnology and Oceanography: Fluids and Environments* **2**, 41-53, doi:10.1215/21573689-1597669 (2012).

34 Wanninkhof, R. Relationship between wind speed and gas exchange over the ocean revisited. *Limnology and Oceanography: Methods* **12**, 351-362, doi:10.4319/lom.2014.12.351 (2014).

35 Sherwood Lollar, B., Hirschorn, S. K., Chartrand, M. M. G. & Lacrampe-Couloume, G. An Approach for Assessing Total Instrumental Uncertainty in Compound-Specific Carbon Isotope Analysis: Implications for Environmental Remediation Studies. *Anal. Chem.* **79**, 3469-3475, doi:10.1021/ac062299v (2007).

36 Davie, M. K. & Buffett, B. A. A numerical model for the formation of gas hydrate below the seafloor. *J. Geophys. Res.* **106**, 497-514, doi:10.1029/2000JB900363 (2001).

37 Tedesco, M. *et al.* Evidence and analysis of 2012 Greenland records from spaceborne observations, a regional climate model and reanalysis data. *The Cryosphere* **7**, 615-630, doi:10.5194/tc-7-615-2013 (2013).

38 Palmer, S., Shepherd, A., Nienow, P. & Joughin, I. Seasonal speedup of the Greenland Ice Sheet linked to routing of surface water. *Earth and Planetary Science Letters* **302**, 423-428, doi:https://doi.org/10.1016/j.epsl.2010.12.037 (2011).

39 Lindbäck, K. *et al.* Subglacial water drainage, storage, and piracy beneath the Greenland ice sheet. *Geophysical Research Letters* **42**, 7606-7614, doi:10.1002/2015GL065393 (2015).

40 Dawes, P. R. The bedrock geology under the Inland Ice: the next major challenge for Greenland mapping. *Geological Survey of Denmark and Greenland Bulletin* **17**, 57-60 (2009).

41 Bartholomew, I. *et al.* Seasonal evolution of subglacial drainage and acceleration in a Greenland outlet glacier. *Nature Geosci* **3**, 408-411 (2010).

42 Tedstone, A. J. *et al.* Greenland ice sheet motion insensitive to exceptional meltwater forcing. *Proceedings of the National Academy of Sciences* **110**, 19719-19724, doi:10.1073/pnas.1315843110 (2013).

43 Hawkings, J. *et al.* The Greenland Ice Sheet as a hot spot of phosphorus weathering and export in the Arctic. *Global Biogeochem. Cycles* **30**, 191-210, doi:10.1002/2015GB005237 (2016).

44 MacGregor, J. A. *et al.* A synthesis of the basal thermal state of the Greenland Ice Sheet. *J. Geophys. Res.* **121**, 1328-1350, doi:10.1002/2015JF003803 (2016).

45 Overeem, I. *et al.* Substantial export of suspended sediment to the global oceans from glacial erosion in Greenland. *Nature Geosci* **10**, 859, doi:10.1038/ngeo3046 (2017).

46 Schuster, P. F. Water and sediment quality in the Yukon River basin, Alaska, during water year 2004. Report No. 2006-1258, 75 (2006).

47 Schuster, P. F. Water and sediment quality in the Yukon River basin, Alaska, during water year 2003. Report No. 2005-1397, (2005).

48 Schuster, P. F. Water and sediment quality in the Yukon River basin, Alaska, during water year 2002. Report No. 2005-1199, (2005).

49 Schuster, P. F. Water and sediment quality in the Yukon River basin, Alaska, during water year 2001. (2003).

50 Striegl, R. G., Dornblaser, M. M., McDonald, C. P., Rover, J. R. & Stets, E. G. Carbon dioxide and methane emissions from the Yukon River system. *Global Biogeochem. Cycles* **26**, n/a-n/a, doi:10.1029/2012GB004306 (2012).

51 U.S. Geological Survey. *National Water Information System data available on the World Wide Web (USGS Water Data for the Nation)*, <http://waterdata.usgs.gov/nwis/> (2016).

52 Bussmann, I. Distribution of methane in the Lena Delta and Buor-Khaya Bay, Russia. *Biogeosciences* **10**, 4641-4652, doi:10.5194/bg-10-4641-2013 (2013).

53 Fedorova, I. *et al.* Lena Delta hydrology and geochemistry: long-term hydrological data and recent field observations. *Biogeosciences* **12**, 345-363, doi:10.5194/bg-12-345-2015 (2015).

54 Muster, S., Langer, M., Heim, B., Westermann, S. & Boike, J. Subpixel heterogeneity of ice-wedge polygonal tundra: a multi-scale analysis of land cover and evapotranspiration in the Lena River Delta, Siberia. *Tellus B: Chemical and Physical Meteorology* **64**, 17301, doi:10.3402/tellusb.v64i0.17301 (2012).

55 Barbosa, P. M. *et al.* Diffusive methane fluxes from Negro, Solimões and Madeira rivers and fringing lakes in the Amazon basin. *Limnology and Oceanography*, n/a-n/a, doi:10.1002/lno.10358 (2016).

56 Moreira-Turcq, P., Seyler, P., Guyot, J. L. & Etcheber, H. Exportation of organic carbon from the Amazon River and its main tributaries. *Hydrological Processes* **17**, 1329-1344, doi:10.1002/hyp.1287 (2003).

57 Borges, A. V. *et al.* Divergent biophysical controls of aquatic CO2 and CH4 in the World's two largest rivers. *Scientific Reports* **5**, 15614, doi:10.1038/srep15614 (2015).

58 Sawakuchi, H. O. *et al.* Methane emissions from Amazonian Rivers and their contribution to the global methane budget. *Global Change Biology* **20**, 2829-2840, doi:10.1111/gcb.12646 (2014).

59 Borges, A. V. *et al.* Globally significant greenhouse-gas emissions from African inland waters. *Nature Geosci* **8**, 637-642, doi:10.1038/ngeo2486 (2015).

60 Bates, S. T. *et al.* Examining the global distribution of dominant archaeal populations in soil. *The Isme Journal* **5**, 908, doi:10.1038/ismej.2010.171 (2010).

61 Schloss, P. D. *et al.* Introducing mothur: Open-Source, Platform-Independent, Community-Supported Software for Describing and Comparing Microbial Communities. *Applied and Environmental Microbiology* **75**, 7537-7541 (2009).

62 Kozich, J. J., Westcott, S. L., Baxter, N. T., Highlander, S. K. & Schloss, P. D. Development of a Dual-Index Sequencing Strategy and Curation Pipeline for Analyzing Amplicon Sequence Data on the MiSeq Illumina Sequencing Platform. *Applied and Environmental Microbiology* **79**, 5112-5120 (2013).

63 Fiedler, B. *et al.* In Situ CO2 and O2 Measurements on a Profiling Float. *Journal of Atmospheric and Oceanic Technology* **30**, 112-126, doi:10.1175/JTECH-D-12-00043.1 (2012).

64 Atamanchuk, D. *et al.* Detection of CO2 leakage from a simulated sub-seabed storage site using three different types of pCO2 sensors. *International Journal of Greenhouse Gas Control* **38**, 121-134, doi:https://doi.org/10.1016/j.ijggc.2014.10.021 (2015).

65 Christoffersen, P. *et al.* Cascading lake drainage on the Greenland Ice Sheet triggered by tensile shock and fracture. *Nature Communications* **9**, 1064, doi:10.1038/s41467-018-03420-8 (2018).

66 Hoffman, M. J. *et al.* Greenland subglacial drainage evolution regulated by weakly connected regions of the bed. *Nature Communications* **7**, 13903, doi:10.1038/ncomms13903 (2016).

67 Das, S. B. *et al.* Fracture Propagation to the Base of the Greenland Ice Sheet During Supraglacial Lake Drainage. *Science* **320**, 778 (2008).

68 Nienow, P., Sharp, M. & Willis, I. Seasonal changes in the morphology of the subglacial drainage system, Haut Glacier d'Arolla, Switzerland. *Earth Surface Processes and Landforms* **23**, 825-843, doi:10.1002/(SICI)1096-9837(199809)23:9<825::AID-ESP893>3.0.CO;2-2 (1998).

69 Stevens, L. A. *et al.* Greenland supraglacial lake drainages triggered by hydrologically induced basal slip. *Nature* **522**, 73, doi:10.1038/nature14480 (2015).

70 Tranter, M. *et al.* Geochemical weathering at the bed of Haut Glacier d'Arolla, Switzerland—a new model. *Hydrological Processes* **16**, 959-993, doi:10.1002/hyp.309 (2002).

71 Lawson, E. C. *et al.* Greenland Ice Sheet exports labile organic carbon to the Arctic oceans. *Biogeosciences* **11**, 4015-4028, doi:10.5194/bg-11-4015-2014 (2014).

72 Lofton, D. D., Whalen, S. C. & Hershey, A. E. Effect of temperature on methane dynamics and evaluation of methane oxidation kinetics in shallow Arctic Alaskan lakes. *Hydrobiologia* **721**, 209-222, doi:10.1007/s10750-013-1663-x (2014).

73 Yvon-Durocher, G. *et al.* Methane fluxes show consistent temperature dependence across microbial to ecosystem scales. *Nature* **507**, 488, doi:10.1038/nature13164 (2014).

74 Souchez, R. *et al.* Gas isotopes in ice reveal a vegetated central Greenland during ice sheet invasion. *Geophysical Research Letters* **33**, n/a-n/a, doi:10.1029/2006GL028424 (2006).

75 Dow, C. F. *et al.* Seismic evidence of mechanically weak sediments underlying Russell Glacier, West Greenland. *Annals of Glaciology* **54**, 135-141, doi:10.3189/2013AoG64A032 (2013).

76 Kulessa, B. *et al.* Seismic evidence for complex sedimentary control of Greenland Ice Sheet flow. *Science Advances* **3** (2017).

77 Ryser, C. *et al.* Caterpillar-like ice motion in the ablation zone of the Greenland ice sheet. *J. Geophys. Res.* **119**, 2258-2271, doi:10.1002/2013JF003067 (2014).

78 Harper, J. T., Humphrey, N. F., Meierbachtol, T. W., Graly, J. A. & Fischer, U. H. Borehole Measurements Indicate Hard Bed Conditions, Kangerlussuaq Sector, Western Greenland Ice Sheet. *J. Geophys. Res.*, n/a-n/a, doi:10.1002/2017JF004201 (2017).